Andean Geology 41 (3): 529-557. September, 2014
doi: 10.5027/andgeoV41n3-a03

Andean Geology
formerly Revista Geológica de Chile
www.andeangeology.cl

The Upper Jurassic volcanism of the Río Damas-Tordillo Formation (33°- 35.5°S): Insights on petrogenesis, chronology, provenance and tectonic implications

Pablo Rossel[1, 8], *Verónica Oliveros[1], José Mescua[2], Felipe Tapia[3], Mihai N. Ducea[4, 5], Sergio Calderón[3, 6], Reynaldo Charrier[3, 7], Derek Hoffman[4]

[1] *Departamento Ciencias de la Tierra, Universidad de Concepción, Casilla 160-C, Concepción, Chile.*
pabrossel@udec.cl; voliveros@udec.cl
[2] *Instituto Argentino de Nivología, Glaciología y Ciencias Ambientales (IANIGLA), CCT Mendoza, CONICET. Avda. Ruiz Leal s/n, Parque General San Martín, Mendoza (5500), Argentina.*
jmescua@mendoza-conicet.gob.ar
[3] *Departamento de Geología, Universidad de Chile, Plaza Ercilla # 803, Santiago, Chile.*
ftapiasilva@gmail.com; rcharrie@ing.uchile.cl
[4] *Department of Geosciences, University of Arizona, Tucson, AZ 85721, USA.*
ducea@email.arizona.edu; mantis@email.arizona.edu
[5] *Universitatea Bucuresti, Facultatea de Geologie Geofizica, Strada N. Balcescu Nr 1, Bucuresti, Romania.*
[6] *Escuela de Ciencias de la Tierra, Universidad Andrés Bello, Quillota 980, Viña del Mar, Chile.*
sergio.calderon@unab.cl
[7] *Escuela Ciencias de la Tierra, Universidad Andrés Bello, Campus República, Avenida República 237, Santiago, Chile.*
rcharrier@unab.cl
[8] *Present address: Facultad de Ingeniería, Geología, Universidad Andrés Bello, Autopista Concepción-Talcahuano 7100, Concepción, Chile.*
pablo.rossel@unab.cl

* *Corresponding author: voliveros@udec.cl*

ABSTRACT. The uppermost Jurassic continental and volcanic deposits of the Río Damas-Tordillo Formation represent an interval of intense continental deposition within the Jurassic to Early Cretaceous dominantly marine environment of the Mendoza-Neuquén back-arc basin. Stratigraphic and geochronological data indicate that progressive emersion of the arc and forearc domain, disconnecting the back-arc region from the Pacific Ocean, occurred during occurred during the Late Jurassic and probably the Early Cretaceous (~160-140 Ma). This change in the margin configuration induced a marine regression and the subsequent deposition of continental material in the back-arc basin. The most likely source of the sediments would have been the Jurassic arc, located west of the back-arc basin. The maximum depositional age of 146.4±4.4 Ma obtained from a red sandstone immediately below volcanic rocks confirms recent Tithonian maximum depositional ages assigned to the Río Damas-Tordillo Formation, and suggests that the volcanic rocks, overlain by marine fossiliferous Tithoninan-Hauterivian sequences, should have erupted within a short time span during the Late Jurassic. Volcanism was probably facilitated by the presence of extensional structures related to the formation of the back-arc basin. Elemental and isotopic data, along with forward AFC models, suggest a depleted sub-arc asthenospheric mantle source for the volcanic rocks and the fractionation of olivine and plagioclase, along with small volumes of lower crust assimilation, as the main processes involved in the magmatic evolution. It is not possible to establish a different source and petrogenetic conditions for the Río Damas-Tordillo Formation and the magmatism in the arc domain located further west, at the present-day Coastal Cordillera.

Keywords: Jurassic, Volcanism, Central Chile, Detrital zircons, Isotopes.

RESUMEN. El volcanismo jurásico superior de la Formación Río Damas-Tordillo (33°-35,5°S): antecedentes su sobre petrogénesis, cronología, proveniencia e implicancias tectónicas. Los depósitos continentales y volcánicos del Jurásico tardío, pertenecientes a la Formación Río Damas-Tordillo, representan un período de intensa sedimentación continental dentro del registro mayormente marino observado en la Cuenca Neuquina, durante el Jurásico y Cretácico Inferior. Datos estratigráficos y geocronológicos indican una progresiva emersión del dominio de arco y antearco, desconectando finalmente a la cuenca de trasarco del Océano Pacífico durante el Jurásico Superior. Este cambio en la configuración del margen tuvo como resultado el desarrollo de una regresión marina y posterior sedimentación continental en la cuenca de trasarco. La fuente de sedimentos más probable habría sido el arco jurásico, ubicado hacia el oeste de la cuenca. La edad máxima de 146,4±4.4 Ma, obtenida en una arenisca roja inmediatamente por debajo de las rocas volcánicas, confirma las edades máximas de depósito titonianas, asignadas recientemente a la Formación Río Damas-Tordillo, y sugiere que las rocas volcánicas cubiertas por secuencias marinas fosilíferas del Titoniano-Hauteriviano fueron emplazadas en un período muy restringido hacia fines del Jurásico. Este volcanismo probablemente fue facilitado por la presencia de estructuras extensionales relacionadas con el desarrollo de la cuenca de trasarco. Datos geoquímicos elementales e isotópicos, junto con modelamientos de ACF, sugieren un manto astenosférico deprimido como fuente del material ígneo, y el fraccionamiento de olivino y plagioclasa, combinado con pequeños volúmenes de asimilación de corteza inferior, como los principales procesos involucrados en la evolución de los magmas. No es posible diferenciar, en términos geoquímicos, la fuente y los procesos petrogenéticos del volcanismo jurásico reconocido en la cordillera de la Costa y el de la Formación Río Damas-Tordillo.

Palabras clave: Jurásico, Volcanismo, Chile central, Circones detríticos, Isótopos.

1. Introduction

The voluminous magmatism developed during the Jurassic and Early Cretaceous in the Coastal Cordillera from southern Perú to central Chile, was mainly produced during a period of active subduction and extensional/transtensional tectonics (Creixell *et al*., 2006, 2009, 2011; Grocott and Taylor, 2002; Oliveros *et al.,* 2006, 2007; Schueber and González, 1999). Subduction of the cold and dense Phoenix plate under the South American continent resulted in roll-back of the oceanic plate, constant outboard migration of the trench, thinning of the continental crust and the development of a N-S trending paleogeography (Charrier *et al*., 2007; Mpodozis and Ramos, 2008). This period was characterized by a magmatic arc emplaced in the present-day Coastal Cordillera and extensive back-arc basins to the east (Charrier *et al*., 2007; Martínez *et al*., 2012; Vicente, 2006), where much more restricted volcanic activity took place (Rossel *et al*., 2013).

The main arc domain has been widely studied in the past decades (Creixell *et al*., 2006, 2009, 2011; Kramer *et al*., 2004; Lucassen *et al*., 2006; Oliveros *et al*., 2006, 2007; Parada *et al.,* 1999; Vergara *et al*., 1995) in order to constrain the genesis and sources of this important magmatic province. Recently Rossel *et al*. (2013) have studied the genesis of back-arc volcanism in northern Chile and Oliveros *et al*. (2012) the features of the non-marine back-arc deposits in the same region.

In Central Chile, the Jurassic arc domain is represented by the Lower Jurassic Ajial Formation and the Upper Jurassic Horqueta Formation. The first is predominantly composed by acidic volcanic lavas and pyroclastic rocks, deposited under alternate marine and continental conditions, while on the other hand the Horqueta Formation is a sedimentary-volcanic unit deposited under continental conditions, with mostly acidic lavas and pyroclastic rocks at the base that grade to intermediate to basaltic lavas to the top of the unit (Vergara *et al.,* 1995).

The sedimentary beds of the Río Damas and Tordillo Formations represent the Upper Jurassic continental back-arc deposits, cropping out in the Principal Cordillera of central Chile and Argentina, respectively. These sequences have been studied in detail in terms of their depositional and tectonic environment (Davidson and Vicente, 1973; Legarreta, 1976; López-Gómez *et al*., 2009; Mescua *et al*., 2008; Naipauer *et al*., 2012, 2014; Spalletti *et al*., 2008; Thiele, 1980; Yrigoyen, 1979; Zavala *et al*., 2008). In contrast, the volcanic deposits within these units are relatively unexplored and their petrogenesis remains undetermined. In particular, it is not clear whether the volcanism represents an eastern part of the main volcanic arc or a retro-arc belt within the back-arc basin.

Below, we present a new set of whole-rock elemental and isotopic data for the volcanic rocks as well as new geochronological results for the sedimentary rocks of the Río Damas-Tordillo Formation, which

allow to better understand the stratigraphic position, sources, evolution and tectonic setting of the volcanism developed close to the Jurassic-Cretaceous boundary in the Principal Cordillera of Chile and Argentina, between 33° and 35.5°S. The Upper Jurassic units were sampled at two localities close to the Chile-Argentina border, the Río Volcán and the Termas del Flaco-Las Leñas areas (Fig. 1) where the volcanic and sedimentary rocks of the Río Damas-Tordillo Formation crop out in continuous sections.

2. Geological Setting

Within the context of the mainly extensional/transtensional tectonics recognized for the arc and back-arc domains in northern and central Chile and Argentina during the Jurassic (Creixell *et al*., 2006, 2009, 2011; Grocott and Taylor, 2002; Legarreta and Uliana, 1999; Scheuber and González, 1999) it is possible to identify two transgression-regression cycles during Jurassic and Early Cretaceous times. The red continental clastic deposits of the Kimmeridgian-Tithonian Río Damas-Tordillo Formation (33 to 35,5°S; Figs. 1, 2 and 3) reflect the transition between: **(a)** the culmination of the first Jurassic transgression-regression event, and **(b)** the initiation of the second one, which began in the Tithonian with the reactivation of normal faults that participated in the early development of the backarc basin extension (tectonic subsidence) associated with volcanism and very coarse breccia deposits (Charrier *et al.,* 2007). Thus, the lavas contained in the Río Damas-Tordillo Formation represent

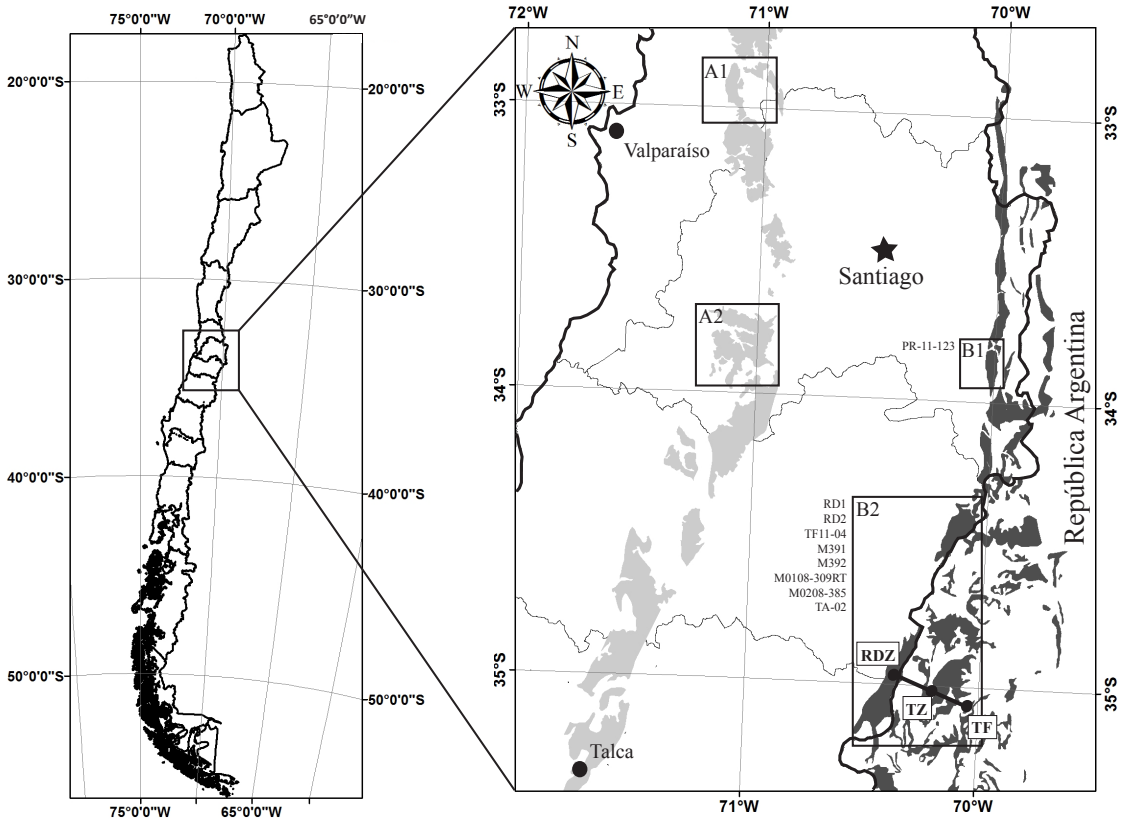

FIG. 1. Simplified geological map of the studied area, showing the location of the relevant units. The gray areas represent the outcrops of the Jurassic volcanic rocks assigned to the arc domain (Ajial and Horqueta formations) and the dark gray areas represent the outcrops of Río Damas and Tordillo Formations. **A1.** Ajial and Horqueta formations and **A2.** Horqueta Formation sampling zones of Vergara *et al.,* 1995; **B1.** Río Volcán area; **B2.** Termas del Flaco and Paso Vergara-Cordón del Burrero area. **RDZ:** Río Damas Zone; **TZ:** Transition Zone; **TF:** Tordillo Formation Zone. Modified after SERNAGEOMIN (2003) and Caminos *et al.* (1993).

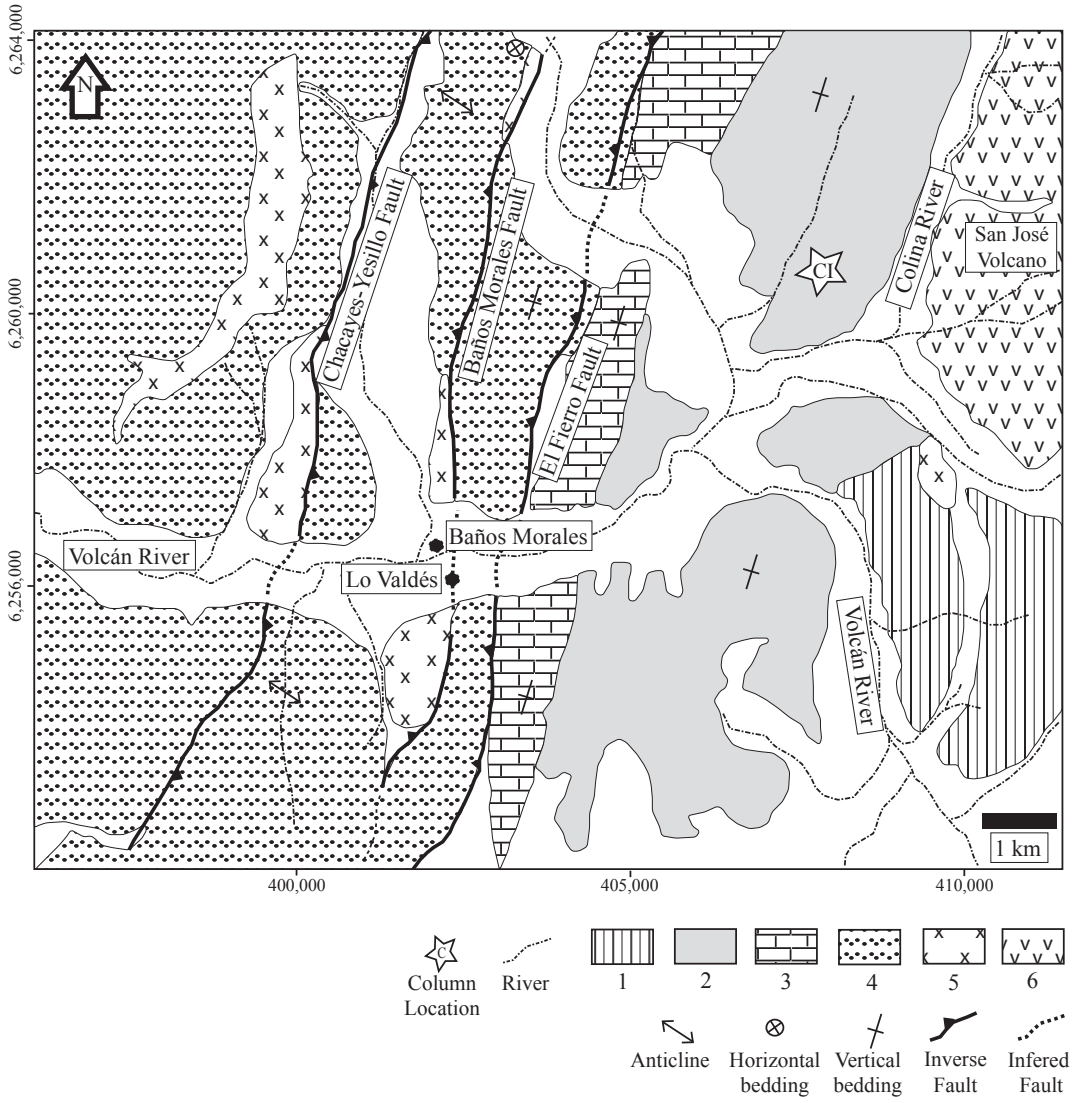

FIG. 2. Simplified geological map of the Río Volcán area (B1 in Fig. 1). Stars show the location of sections in figure 5. **1.** Río Colina Formation; **2.** Río Damas-Tordillo Formation; **3.** Lo Valdés Formation; **4.** Cenozoic volcano-sedimentary deposits; **5.** Miocene intrusives; **6.** Quaternary volcanism. Modified after Calderón (2008).

a particular event of volcanic activity, accompanied by continental sedimentation, that took place during the latest Jurassic-earliest Cretaceous in the western border of the Mendoza-Neuquén Basin (Mescua, 2011; Fig. 4). The volcanic deposits are interpreted as either the distal components of the main volcanic arc developed to the west in the present-day Coastal Cordillera (Davidson, 1971; Davidson and Vicente; 1973), or back-arc volcanism emplaced through the normal faults that accommodated the extension in the back-arc basin (Charrier *et al*., 2007). The back-arc volcanism would have occurred also during the Early Cretaceous, since volcanic intercalations have been found within the marine Tithonian-Hauterivian Lo Valdés and Baños del Flaco formations, which overlie the Río Damas Formation in this same region (González, 1963; Biro-Bagoczky, 1964), between 33º30'S and 34º15'S.

In the Río Volcán area, close to La Valdés village, the Río Damas Formation (Klohn, 1960; Figs. 2 and 5)

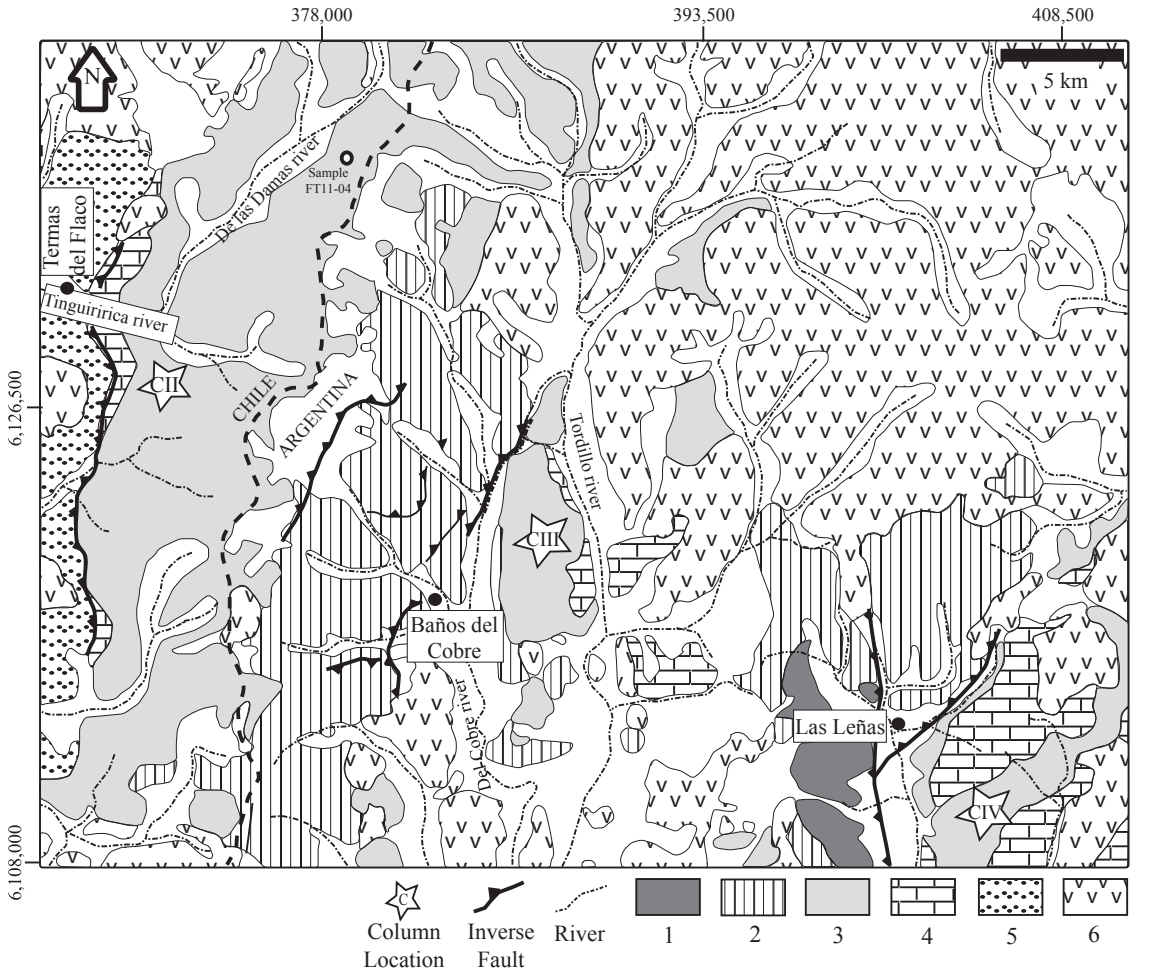

FIG. 3. Simplified geological map of the Termas del Flaco-Las Leñas area (B2 in Fig. 2). Stars show the location of sections in figure 5. **1.** Choiyoi rocks; **2.** Jurassic marine sediments; **3.** Río Damas-Tordillo Formation; **4.** Post-Tithonian marine deposits; **5.** Cenozoic volcano-sedimentary deposits; **6.** Quaternary volcanism. Modified after Mescua (2011).

concordantly overlies Callovian-Oxfordian marine and evaporitic deposits of the Río Colina Formation (González, 1963), composed mainly by limestones, calcareous shales, sandstones and conglomerates with minor intercalations of lavas, and important levels of gypsum, and underlies the marine deposits of the Lo Valdés Formation (González, 1963), which comprises by over 1,000 m of marine fosiliferous deposits of Tithonian-Hauterivian age, with intercalated hialoclastic andesites (Hallam *et al*., 1986; Thiele, 1980). In this area the Río Damas Formation is represented by a basal level (3 to 10 m) of massive coarse sandstones that underlies a series of andesitic lava flows with a maximum thickness of 500 m. To the top the lavas become more brecciated and are overlied by a series of clastic continental conglomerates and breccias that contain abundant volcanic clasts of the andesitic lava flows (Fig. 5).

At its type locality, close to Termas del Flaco area (Fig. 3), the Río Damas Formation consists of a *ca*. 3,000-m-thick continental succession of red beds, with intercalations of coarse- and fine-grained rocks, that includes at the top >1,000 m of andesitic lavas and volcanic breccias with large angular blocks, some over 4 m in diameter (Charrier *et al*., 1996), and underlies the marine deposits of the Termas del Flaco Formation of Tithonian age (Klohn, 1960; Fig. 5). To the east, the Río Damas

Formation interfingers the clastic continental rocks of the Tordillo Formation (Stipanicic, 1969; Fig. 5), mainly red sandstones with conglomerates and shales that are representative of fluvial, eolian, alluvial and playa lake environments (Legarreta *et al*., 1993).

South of 35,5°S, the Río Damas Formation overlays the gypsum deposits of Santa Elena Formation located on top of Nacientes del Teno Formation (Davidson, 1971; Davidson and Vicente, 1973).

The Tordillo Formation, which is the Argentinean equivalent to the Río Damas Formation, concordantly overlies in concordance the evaporitic deposits of the Auquilco Formation (Stipanicic, 1965), composed mainly by gypsum, anhydrite and minor limestones of Oxfordian age, with a maximum thickness of 400 m, and underlies in concordance the marine deposits of the Vaca Muerta Formation (Weaver, 1931), which represent a new marine flooding in the back-arc basin, evidenced by deposits of black shales and fosiliferous limestones of Tithonian-Berriasian age.

As show in figure 4, the deposits of the Río Damas-Tordillo Formation represent a main event of emersion of the back-arc basin that took place during the Kimmeridgian. A decrease in the proportion of volcanic rocks from west to east suggests that the contribution of volcanic material is mainly from the west (Fig. 5). These units present abrupt changes in thickness in the studied area. A main depocenter was located in the western part of the basin, controlled by active extensional faults (Mescua, 2011; Mescua *et al*., 2008), confirming the existence of very active tectonics during this period of the Jurassic.

The deposits of the Río Damas-Tordillo Formation are tilted and deformed as a consequence of

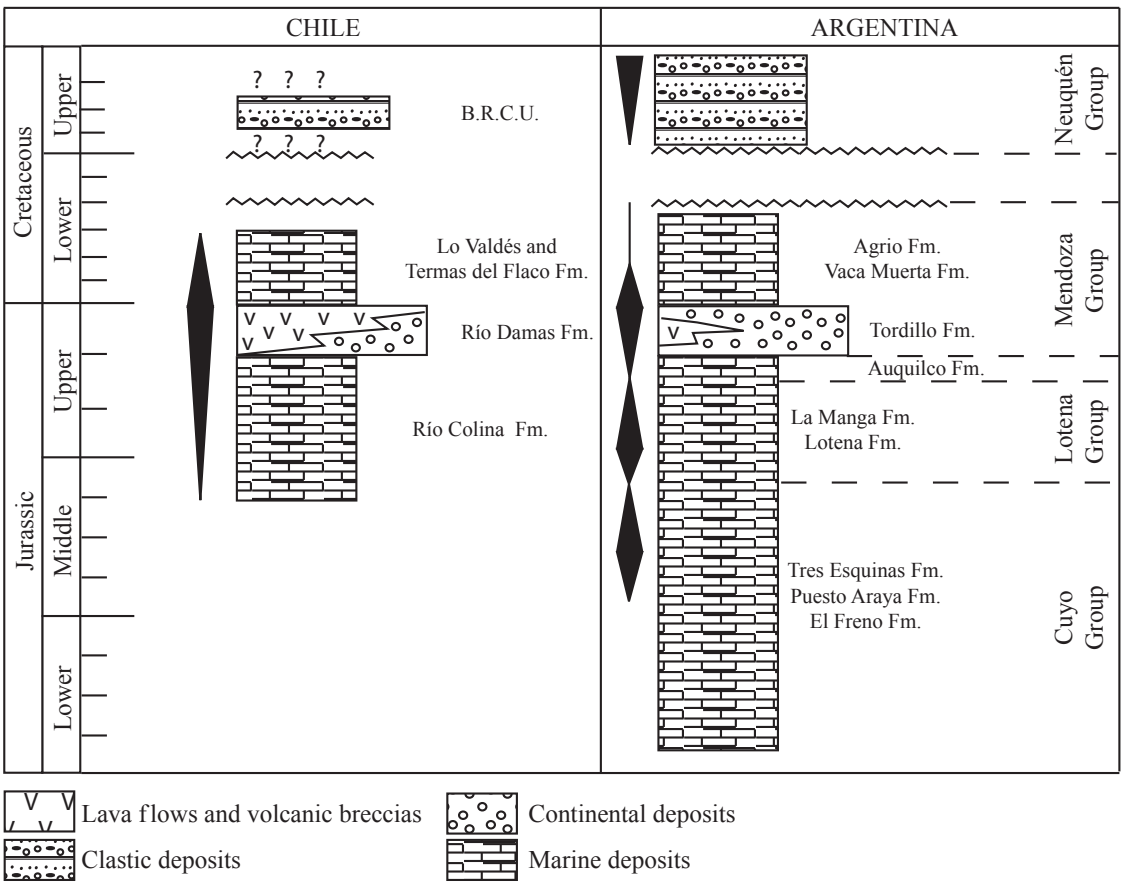

FIG. 4. Tectonostratigraphic chart of the Jurassic to Lower Cretaceous back-arc sequences cropping out in the studied areas in Chile (Río Volcán and Baños del Flaco) and Argentina (Loma de las Vegas and East of Valle de Las Leñas).

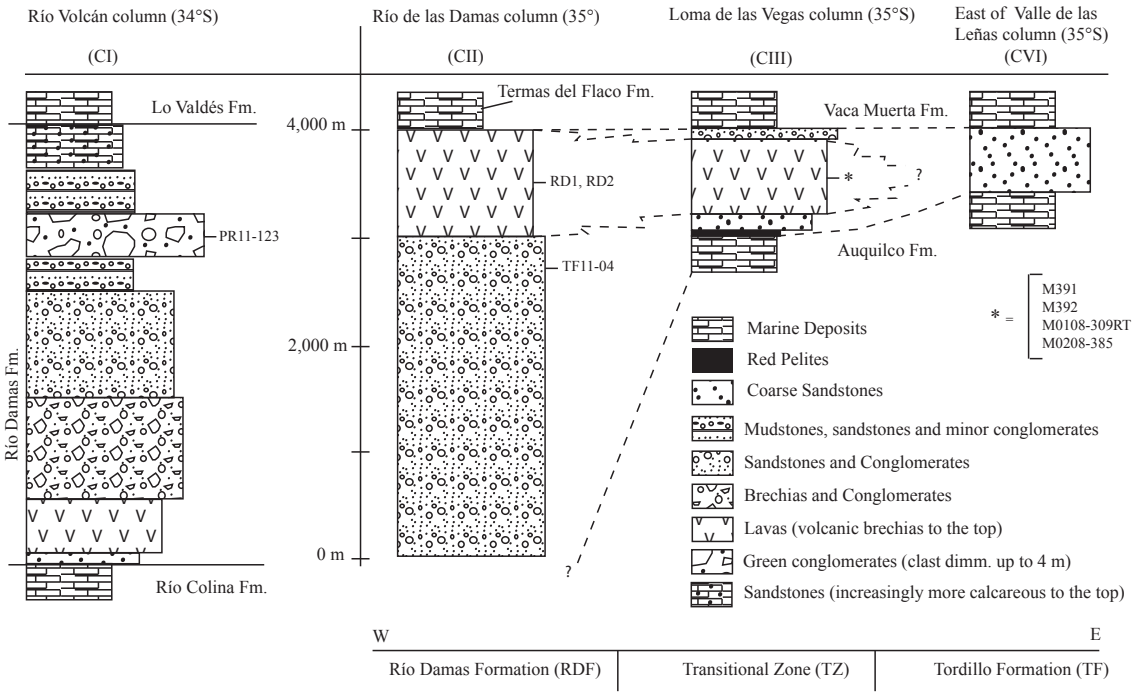

FIG. 5. Schematic sections of the Río Damas-Tordillo Formation at the sampling locations, showing the stratigraphic position of the continental deposits at 34° and 35°S, and their lateral variations at 35°S. Transitional zone is equivalent to the 'lateral intercalation zone' defined by Mescua (2011). Thickness of the restored sections are reported in the work of Calderón (2008) for the Río Volcán area, Charrier *et al.* (1996) for the Termas del Flaco area and Mescua (2011) for the Loma de las Vegas and east of Valle de Las Leñas areas. Note the thickness of the breccias and conglomerates beds at the top of Río Volcán section in contrast to the scarce clastic material in the Termas del Flaco section.

the developement of the Andean fold and thrust belt. In the studied areas (Figs. 2 and 3), the Río Damas Formation crops out in the backlimb of great anticlines of 10 km of wavelength, and the beds have moderate to high dips, being locally subvertical. The Tordillo Formation crops out in smaller folds (5 to 1 km wavelength), with dips under 45°. A major unconformity separates Mesozoic units from the much less deformed Cenozoic deposits (Charrier *et al*., 2007; Mescua *et al*., 2012).

3. Petrography of the Río Damas-Tordillo Formation Volcanic Components

The volcanic rocks of the Río Damas-Tordillo Formation are mainly red brownish to dark purple porphyric, sometimes vesicular, lava flows and sills. Intercalations of volcanic breccias bearing fragments of andesitic lavas of 1 to 4 m in size and more fine grained pyroclastic deposits can be found along the frontier of Chile and Argentina. The samples analyzed in this work correspond mainly to basaltic andesites and minor andesites.

3.1. Petrography of the primary components

The studied lavas have a porfiric texture, with up to 35% of phenocrysts content. Euhedral plagioclase phenocrysts up to 4 cm in size represent *ca.* 70% of the phenocrysts content of the rocks. Precise petrographic determination of their composition is difficult because of the alteration. However, the Michell-Levy method was applied to eight single crystals in one fresh sample (sample M391, figure 5), indicating that the plagioclases are andesine in composition (An_{38}). 25% of the phenocrysts correspond to eu- and sub-hedral clinopyroxene crystals; and the remaining 5% of the phenocyrsts are Fe-Ti oxides, mostly magnetite with subordinate ilmenite. The groundmass has an intersertal texture and it is composed of plagioclase microlites, Fe-Ti oxides and alteration minerals.

3.2. Petrography of the alteration components

All the volcanic and sedimentary rocks of the Río Damas-Tordillo Formation are altered to some extent, as a consequence of burial and contact metamorphism (Calderón, 2008; Levi *et al.,* 1989; Oliveros *et al.,* 2008; Robinson *et al.,* 2004). The alteration in general is very penetrative, partly hiding the primary features of the rock, particularly at the contact between beds, vesicular portions or highly fractured zones of the lava flows and in the fine matrix of volcanic and sedimentary rocks. Central portion of lava flows or restricted domains within the sedimentary rocks are often less affected by the alteration processes. The observed alteration minerals are: prehnite, pumpeyllite, chlorite, epidote, titanite, actinolite, calcite, quartz, white mica (sericite), albite and K-feldspar, defining a typical mineralogy of prenhite-pumpeyllite facies in concordance with the reported by others authors for this Andean region (Calderón, 2008; Levi *et al.,* 1989; Oliveros *et al.,* 2008; Robinson *et al.,* 2004). The fine grained volcanic litharenites from the easternmost outcrops of the Río Damas Formation, in the head of the Maipo river valley at 34º15'S, bear scarce calcite and chlorite as secondary mineral phases, indicating that the alteration degree diminishes eastward (Charrier, 1981).

Plagioclase phenocrysts, microlites and fragments in the volcanic rocks are partial to completely replaced by a mixture of sericite, clays and minor albite and epidote. The clinopyroxenes are often completely replaced by chlorite and titanite, but fresh phenocrysts can be observed in the central part of the lava flows. The components of the matrix or groundmass are often replaced by chlorite, titanite and clays. Finally, the vesicles of the lavas are filled with calcite, quartz, prehnite, pumpeyllite, and it is possible to recognize multiple stages of mineral formation.

4. Samples and Methods

Seven slightly altered lava samples, one sample of sandstone and one sample of a granitic clast from a polymitic sedimentary breccia of the Río Damas-Tordillo Formation were collected for analysis (Fig. 1).

4.1. Whole rock analysis

Major and trace element concentrations were determined using standard XRF and ICP-MS techniques at University of Arizona. Major elements were performed on a HORIBA XRF instrument on powdered pressed pellets; analytical precision is about 2% of the reported value. Whole-rock trace elements were measured in solution using a Thermo Element X-Series II single collector ICP-MS at the University of Arizona (Rossel *et al.,* 2013). Approximately 5 mg of sample were dissolved in about 7 ml of concentrated HF-HNO_3 mixtures, dried down and redissolved in a mild 1% nitric acid before being analyzed. Several 1-10 ppm internal standards were used for different elements. Columbia River Basalt material standard material was used as an external standard. Analysis routines involved 30 individual measurements of isotopes free of interferences. Typical analytical errors are 3-5% of the reported values.

Sr and Nd isotopic analyses were performed at the University of Arizona (following procedures outlined in Otamendi *et al.,* 2009) on a VG Sector 54 multicollector TIMS instrument, the Sr isotopic ratios were normalized to $^{86}Sr/^{88}Sr=0.1194$, whereas the Nd isotopic ratios were normalized to $^{146}Nd/^{144}Nd=0.7219$. Estimated analytical $\pm 2\sigma$ uncertainties are: $^{87}Sr/^{86}Sr=0.001\%$ and $^{143}Nd/^{144}Nd=0.001\%$. Ten analyses of standard SRM 987 analyzed during the course of this study yielded mean ratios of $^{87}Sr/^{86}Sr=0.710264\pm7$ and six analyses of Nd standard La Jolla Nd yielded a mean ratio of $^{143}Nd/^{144}Nd=0.511848\pm11$. Procedural blanks averaged from five determinations were: Sr-150 pg, and Nd-5.5 pg.

The common isotopes of Pb were analyzed on the sample aliquots from which Rb-Sr and Sm-Nd isotopes were analyzed following the procedures described in Drew *et al.* (2009). Separate batches of dissolved samples were saved for lead chemistry. Pb was extracted on Sr-spec columns (Drew *et al.,* 2009). Lead isotope analysis was conducted on a GV Instruments multicollector inductively coupled plasma mass spectrometer (MC-ICP-MS) at the University of Arizona (Thibodeau *et al.,* 2007). Samples were introduced into the instrument by free aspiration with a low-flow concentric nebulizer into a water-cooled chamber. A blank, consisting of 2% HNO_3, was run before each sample. Before analysis, all samples were spiked with a Tl solution to achieve a Pb/Tl ratio of ~10. Throughout the experiment, the standard National Bureau of Standards(NBS)-981 was run to monitor the stability of the instrument.

4.2. U-Pb geochronology of igneous and detrital zircons

Zircons were extracted from a granitic clast in a sedimentary breccia (PR-11-123) and from a sandstone (TF11-04) by crushing, milling, gravitational separation and heavy liquids treatment. At least 50 crystals were randomly selected (regardless their size, form or color) using a stereomicroscope and then mounted in 25 mm epoxy and polished.

U-Pb geochronology of zircons was conducted by LA-MC-ICP-MS at the Arizona LaserChron Center (Gehrels *et al*., 2008). The analyses involve ablation of zircon with a New Wave/Lambda Physik DUV193 Excimer laser (operating at a wavelength of 193 nm) using a spot diameter of 25 or 35 μm. The ablated material is carried with helium gas into the plasma source of a GV Instruments Isoprobe, which is equipped with a flight tube of sufficient width that U, Th, and Pb isotopes are measured simultaneously. All measurements were made in static mode, using Faraday detectors for ^{238}U and ^{232}Th, an ion-counting channel for ^{204}Pb, and either Faraday collectors or ion counting channels for $^{208–206}Pb$. Ion yields are ~1 mV ppm^{-1}. Each analysis consists of one 20 s-integration on peaks with the laser off (for backgrounds), twenty 1 s-integrations with the laser firing, and a 30 s delay to purge the previous sample and to prepare for the next analysis. The ablation pit is ~15 μm in depth.

For each analysis, the errors in determining $^{206}Pb/^{238}U$ and $^{206}Pb/^{204}Pb$ result in a measurement error of ~1% (at 2σ level) in the $^{206}Pb/^{238}U$ age. The errors in measurement of $^{206}Pb/^{207}Pb$ and $^{206}Pb/^{204}Pb$ also result in ~1% (2σ) uncertainty in age for grains that are >1.0 Ga, but are substantially larger for younger grains due to low intensity of the ^{207}Pb signal. For most analyses, the crossover in precision of $^{206}Pb/^{238}U$ and $^{206}Pb/^{207}Pb$ ages occurs at ~1.0 Ga. Common Pb correction is accomplished by using the measured ^{204}Pb and assuming an initial Pb composition from Stacey and Kramers (1975) (with uncertainties of 1.0 for $^{206}Pb/^{204}Pb$ and 0.3 for $^{207}Pb/^{204}Pb$). The measurement of ^{204}Pb is unaffected by the presence of ^{204}Hg because backgrounds are measured on peaks (thereby subtracting any background ^{204}Hg and ^{204}Pb), and because very little Hg is present in the argon gas. Interelement fractionation of Pb/U is generally ~20%, whereas fractionation of Pb isotopes is generally <2%. In-run analysis of fragments of a large Sri Lanka zircon crystal (generally every fifth measurement) with known age of 564±4 Ma (2σ error) is used to correct for this fractionation (see Gehrels *et al*., 2008). The uncertainty resulting from the calibration correction is generally ~1% (2σ) for both $^{206}Pb/^{207}Pb$ and $^{206}Pb/^{238}U$ ages.

The reported ages are determined from the weighted mean of the $^{206}Pb/^{238}U$ ages of the concordant and overlapping analyses (Ludwig, 2003). The reported uncertainty (labeled 'mean') is based on the scatter and precision of the set of $^{206}Pb/^{238}U$ or $^{206}Pb/^{207}Pb$ ages, weighted according to their measurement errors (shown at 1σ). The systematic error, which includes contributions from the standard calibration, age of the calibration standard, composition of common Pb and U decay constants, is generally ~1-2% (2σ).

5. Results

5.1. Whole Rock Chemistry

The major and trace elements abundances for the studied volcanic rocks are listed in the Table 1.

5.1.1. Alteration

The alteration that affects the Mesozoic and Cenozoic volcano-sedimentary rocks cropping out in the Andes of Central Chile, which can be very pervasive, is the result of the combination of very low-grade burial metamorphism (Prenhite-Pumpellyte facies), and contact metamorphism and hydrothermal alteration related to the intrusion of numerous granitic stocks of Miocene age (Calderón, 2008; Levi *et al.,* 1989; Muñoz *et al.,* 2009; Oliveros *et al.,* 2008; Robinson *et al.,* 2004; Thiele, 1980).

Although the studied samples exhibited slight to moderate evidences of alteration, the afore mentioned processes were likely responsible for an increase in the amount of total alkalis as it is inferred from the comparison between the total alkalis *versus* silica classification plot (TAS) and the diagram for altered rocks which plots Zr/Ti *versus* Nb/Y (Fig. 6). In the first diagram, an important number of samples plot in the trachy-andesite and trachy-dacite fields, whereas in the diagram for altered rocks the samples plot in the basalts, basaltic andesites-andesites and dacites-ryolites fields. Therefore, the alkali enrichment of the rocks is likely due to the albitization/sercitizacion of the plagioclase phenocrysts or

microlites and clinopyroxene chloritization, not to magmatic processes. The samples also show higher dispersion for large ion lithophile elements (LILE) than high field strength elements (HFSE) (Fig. 7), suggesting that HFSE are less mobile during alteration processes, and therefore more reliable for determining the petrogenesis of the rocks. The light REE (LREE) are enriched in comparison to the heavy REE (HREE), a pattern that is independent of the alteration degree of the sample (Fig. 7).

The most altered sample is MO208-385. The plagioclase and clinopyroxene phenocrysts are completely replaced by sericite and clays and chlorite, respectively, the matrix is chloritized and the numerous vesicles filled with calcite, chlorite, pumpeyllite, prehnite and quartz. It has low abundances of Ba and Th, and high concentrations of Cs (Table 1). The patterns for the REE and HFSE, are similar to those of the less altered rocks, but in general the concentration of these elements is lower in MO208-385.

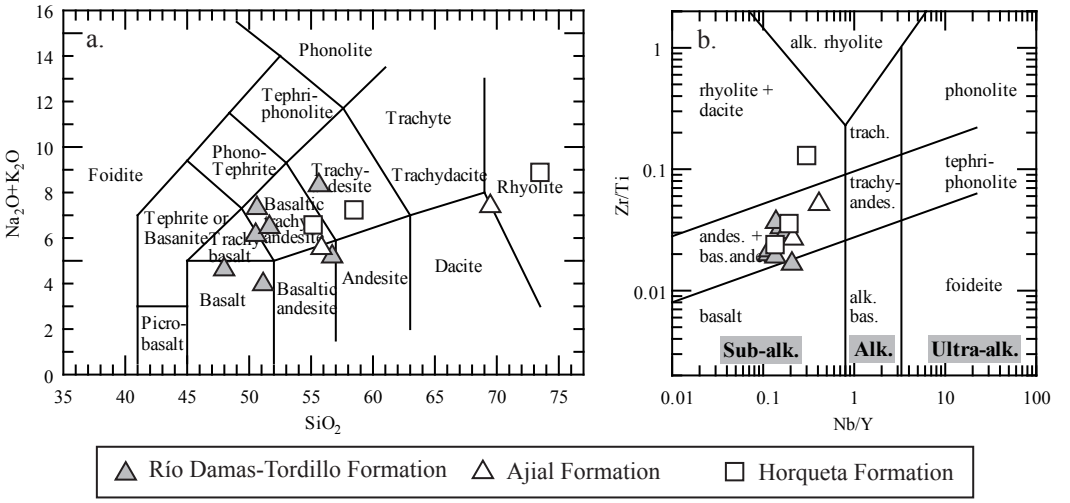

FIG. 6. **a.** Total alkali *versus* silica classification diagram (TAS, Le Maitre, 1989); **b.** Nb/Yb *versus* Zr/Ti classification diagram for altered volcanic rocks (Pearce, 1996 after Winchester and Floyd, 1977). Data from Ajial and Horqueta Formations in the Coastal Cordillera of Central Chile are after Vergara *et al.* (1995).

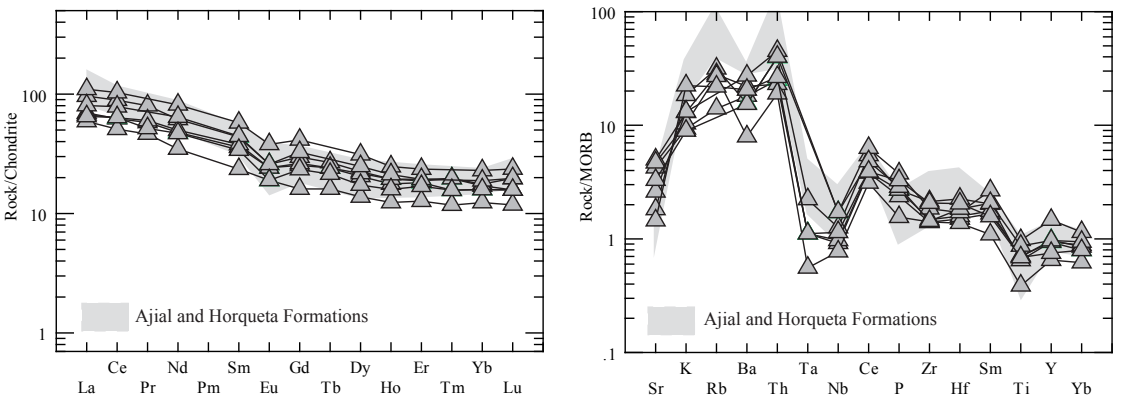

FIG. 7. Chondrite-normalized Rare Earth elements (REE) patterns and MORB-normalized trace elements patterns for volcanic rocks from the Río Damas Formation in the principal cordillera. Data from Ajial and Horqueta Formations in the Coastal Cordillera of Central Chile are after Vergara *et al.* (1995). Normalizing values are from Sun and McDonough (1989) (Chondrite) and Pearce (1983) (MORB).

TABLE 1. MAJOR AND TRACE ELEMENT CHEMISTRY OF UPPER JURASSIC BACK-ARC VOLCANIC ROCKS IN THE STUDIED UNITS.

Área	Cordón del Burrero				Termas del Flaco		Paso Vergara
Sample	M391	M392	M0108-309RT	M0208-385	RD-1	RD-2	TA-02
SiO_2	48.77	55.63	50.58	56.78	51.53	51.11	50.78
TiO_2	1.06	0.97	1.04	0.58	1.46	1.30	1.03
Al_2O_3	17.56	16.60	16.90	17.69	15.91	17.35	15.50
FeO(t)	9.25	6.04	8.78	5.95	11.70	9.32	7.88
MnO	0.11	0.12	0.20	0.14	0.09	0.13	0.19
MgO	4.65	2.30	4.93	4.57	5.42	3.70	4.33
CaO	8.90	4.95	5.50	4.85	1.12	8.75	3.58
Na_2O	3.29	5.78	4.32	3.73	4.71	2.84	4.08
K_2O	1.40	2.76	1.95	1.55	1.97	1.34	3.35
P_2O_5	0.29	0.33	0.33	0.19	0.46	0.35	0.40
LOI	2.88	1.82	3.91	2.40	4.41	2.83	8.78
Total	98.16	97.29	98.44	98.43	98.78	99.02	99.90
#Mg	47.26	40.45	50.02	57.80	45.23	41.44	49.46
Rb	28.0	63.0	56.0	54.0	-	-	43.7
Cs	0.3	0.2	-	3.7	-	-	2.4
Pb	12.0	6.0	11.0	-	-	-	3.4
Ba	362.0	312.0	440.0	159.0	546.0	307.0	410.2
Th	5.0	7.9	4.6	3.8	9.0	8.0	5.3
U	1.4	2.2	1.3	1.0	-	-	2.0
Nb	3.2	4.4	3.4	2.7	6.0	6.0	4.0
Ta	0.2	0.4	0.2	0.1	-	-	0.2
Sr	508.0	218.0	598.0	562.0	312.0	395.0	173.9
Zr	126.0	192.0	133.0	127.0	166.0	129.0	186.1
Hf	3.6	5.4	3.8	3.3	4.1	4.4	4.9
Sc	32.0	28.0	29.0	16.0	35.0	27.0	10.2
V	284.0	246.0	275.0	145.0	338.0	278.0	159.6
Cr	-	40.0	-	-	8.0	3.0	37.3
Ni	-	-	-	-	9.0	7.0	21.0
Zn	80.0	50.0	170.0	60.0	361.0	111.0	159.7
Y	28	28.2	29.2	19.5	44	29	22.5
La	16.5	22.8	15.9	14.0	26.0	19.0	15.4
Ce	38.1	54.4	38.8	31.1	63.0	48.0	39.0
Pr	5.5	7.6	5.7	4.4	-	-	4.9
Nd	22.3	28.7	23.3	16.2	38.0	30.0	21.9
Sm	5.5	6.7	5.8	3.6	8.8	6.8	5.2
Eu	1.4	1.5	1.4	1.1	2.2	1.5	1.1
Gd	5.2	6.1	5.4	3.3	8.5	6.7	4.8
Tb	0.9	1.0	0.9	0.6	-	-	0.8
Dy	5.2	5.7	5.5	3.5	7.9	6.3	4.4
Ho	1.0	1.1	1.1	0.7	1.4	1.2	0.9
Er	3.0	3.1	3.2	2.1	3.9	3.2	2.8
Tm	0.4	0.5	0.5	0.3	-	-	0.4
Yb	2.7	3.0	2.9	2.1	3.9	3.2	2.7
Lu	0.4	0.5	0.4	0.3	0.6	0.5	0.4
ΣREE	108.3	142.6	110.8	83.3	164.2	126.3	104.7

(oxides in wt.%, trace elements in ppm)

5.1.2. Major elements

The SiO_2 content (anhydrous base) in the rocks of the Río Damas-Tordillo Formation varies between 48.77% and 56.78%. The total alkalis vary between 4.28 and 8.54%, although partly due to alteration processes. In general, the lavas have low MgO (2.30-5.42%) and high Al_2O_3 (15.91-17.69%) contents. The #Mg[1] of the rocks varies between 40.45 and 57.80%, indicating differentiation processes in its evolution. The contents of MgO, TiO_2, Al_2O_3, CaO and FeO_t apparently decrease with increasing SiO_2, this is probably related to the fractionation of mineral phases such as magnetite, olivine, plagioclase and clinopyroxene, which are observed in the samples. On the contrary, the alkalis, K_2O and Na_2O, increase with increasing SiO_2, which is due to the incompatible behavior of these elements during the early stages of magma differentiation.

Considering the high dispersion of mayor elements including silica, oxides are not useful as petrogenetic tools in the studied rocks, and they will be only used for comparison purposes in this work.

5.1.3. Trace elements

MORB-normalized multielement spider diagrams exhibit similar patterns for all the studied samples of the Río Damas-Tordillo Formation (Fig. 7), with enrichment in LILE compared to HFSE. The LILE concentrations are quite variable since these elements are more mobile during alteration and incompatible during early stages of crystal fractionation. The lavas have marked negative Nb-Ta-Ti and positive Pb anomalies. Zr and Th have well defined positive correlations with SiO_2 content, but with higher dispersion for Zr. Sr has a high dispersion but apparent negative correlation with SiO_2, probably because of the replacement of CaO during plagioclase fractionation. V has a well defined negative correlation with SiO_2, likely due to fractionation of mineral phases such as magnetite or ilmenite. A similar behavior should be expected for elements like Cr and Ni, although they were not measured in all samples.

Chondrite-normalized REE patterns exhibit a negative slope, with significant enrichment in light REE (LREE) compared to the heavy REE (HREE). Chondrite-normalized La/Yb ratios ($[La/Yb]_n$) range between 4 and 6.The HREE show a rather flat pattern and have abundances between 12 and 23 times the chondritic value. Incipient Eu negative anomalies are present in all the studied rocks, except for the sample MO208-385.

5.1.4. Isotopes

Three samples of the Río Damas-Tordillo Formation were analyzed for Nd, Sr and Pb isotopes; the results are listed in the Table 2.

Nd and Sr isotopic ratios normalized to 150 Ma (Fig. 8a) show values in a restricted range between 0.51282 and 0.51253 and 0.7040 and 0.7044 respectively. On the other hand, the isotopic ratios of Pb ($^{206}Pb/^{204}Pb$=18.57-18.96; $^{207}Pb/^{204}Pb$=15.61-15.64; $^{208}Pb/^{204}Pb$=38.52-39.04) show a wider range (Fig. 8b) of values but still in the range of rocks of the Jurassic volcanic arc of northern Chile (Kramer *et al*., 2004; Lucassen *et al*., 2006).

5.2. U-Pb Geochronology

The results of U-Pb dating of magmatic and detrital zircons in rocks from the Río Damas-Tordillo Formation are listed in Table 3.

TABLE 2. Sr, Nd AND Pb ISOTOPIC COMPOSITION OF RÍO DAMAS-TORDILLO FORMATION VOLCANIC ROCKS.

Sample	$^{87}Sr/^{86}Sr$	$^{87}Sr/^{86}Sr(i)$	$^{143}Nd/^{144}Nd$	$^{143}Nd/^{144}Nd(i)$	εNd	εNd(i)	$^{206}Pb/^{204}Pb$	$^{207}Pb/^{204}Pb$	$^{208}Pb/^{204}Pb$
M391	0.7044	0.7040	0.51318	0.51282	25.40	7.2	18.57	15.61	38.52
M392	0.7061	0.7044	0.51278	0.51253	6.73	1.7	18.77	15.64	38.79
TA-02	0.7057	0.7043	0.51273	0.51258	4.37	2.7	18.96	15.63	39.04

εNd values are calculated as deviations from a chondritic uniform reservoir in part per 104, using present-day values of $^{143}Nd/^{144}Nd$= 0.512638 and $^{147}Sm/^{144}Nd$=0.1967 (Cheng and Wasserburg, 1981; Faure, 1986). Ages of rocks are from an average estimated age of 150 My.

[1] $(MgOwt\%/PM_{MgO})/((MgOwt\%/PM_{MgO})+(FeO^twt\%/PM_{FeO}))*100$

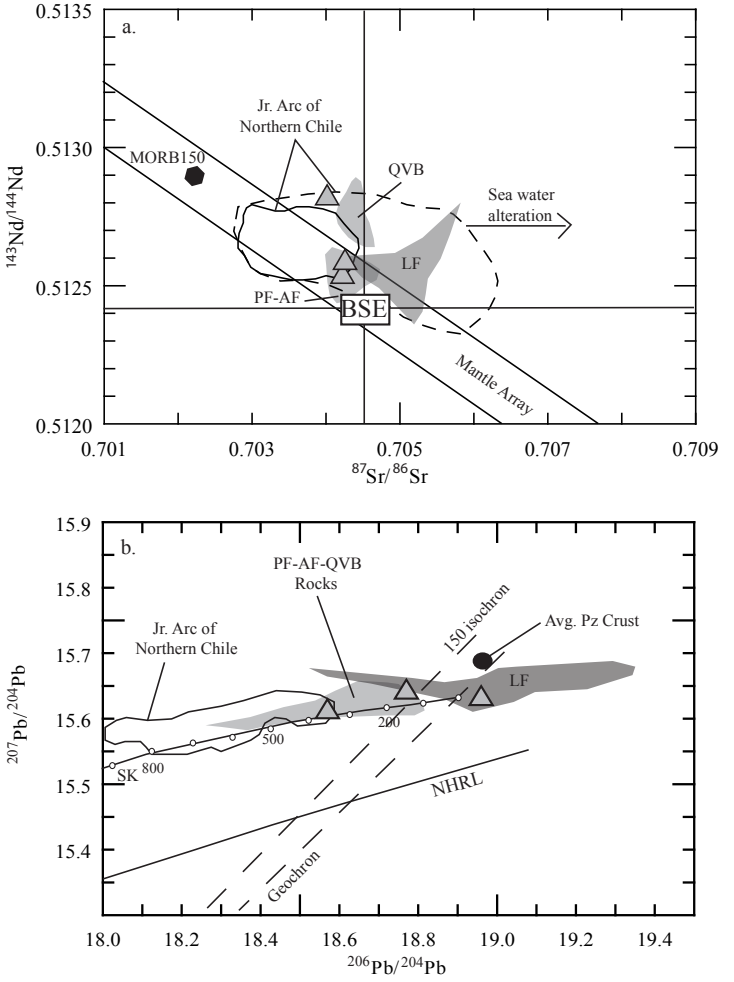

FIG. 8. **a.** $^{87}Sr/^{86}Sr$ *versus* $^{143}Nd/^{144}Nd$ diagram from samples of the Río Damas Formation. **BSE:** Bulk Silica Earth, ages corrected for in situ decay at 150 Ma. Dashed line shows isotopic composition of the Jurassic arc rocks in northern Chile and heavy line shows high density (>95%) of published data these rocks, MORB 150 is actual MORB corrected for *in situ* decay, gray fields are from Upper Jurassic back-arc rocks in northern Chile; **b.** Pb isotopic ratios for volcanic rocks of the Río Damas Formation. **SK:** The Stacey and Kramer (1975) curve of common Pb growth for the average Earth. **NHRL:** Northern Hemisphere Reference Line after Hart (1984); heavy line shows isotopic composition of the Jurassic arc rocks in northern Chile (>90% of published data), gray fields are from Upper Jurassic back-arc rocks in northern Chile. The 150-Ma isochron and the geochron were calculated following the procedures of Stacey and Kramer (1975) and Faure and Mesing (2005); **QVB:** Quebrada Vicuñita Beds: **PF:** Picudo Formation; **AF:** Algarrobal Formation and **LF:** Lagunillas Formation. Arc isotopic data after Kramer *et al.* (2004), Lucassen and Franz (1994), Lucassen *et al.* (2006) and Rossel *et al.* (2013).Upper Jurassic back-arc isotopic data after Rossel *et al.* (2013). Average Paleozoic Crust (Av. Pz Crust) data after Lucassen *et al.* (2002).

Sample PR-11-123 is a granitic fragment extracted from the polimictic breccia in the top of the Río Volcán section (Fig. 5) that yielded a Carboniferous age of 333.1± 6.0 Ma (Fig 9a). The younger analyzed zircons in this sample probably reflect a Pb loss or accidental crystals.

Sample TF11-04 is a red sandstone collected at the top of the sedimentary part in the Termas del Flaco section, but below the volcanic rocks of the sequence (Fig. 5). A total of the 92 zircons grains were analyzed (Table 3). The distribution of the ages is characterized as unimodal with a peaks *ca.* 158 Ma. There are two isolated ages at 415 Ma. The calculated mean age of the youngest five grains, that overlap in age at 2σ, yields a maximun depositational age of 146.4±4.4 Ma (Fig. 9b), for the clastic sediments of the Río Damas-Tordillo Formation in this area.

6. Discussion

6.1. Age and provenance of the Río Damas-Tordillo Formation.

The age of the Río Damas-Tordillo Formation has been commonly assigned to the Kimmeridgian based on its stratigraphic position between Oxfordian and Tithonian-Huaterivian marine fossiliferous deposits (Klohn, 1960; Legarreta y Uliana, 1999; Thiele, 1980). However, the maximum Late Tithonian depositional age of 146.4±4.4 Ma obtained on the base of the youngest group of zircons with concordant ages in sample TF11-04, which underlies the volcanic succession at the Río de las Damas area, is younger than the age constrained by the fossiliferous content of the lowest part of the overlying Lo Valdés, Baños

TABLE 3. SUMMARY OF U-Pb LA-MC-ICP-MS DATA FOR DETRITAL ZIRCON. PREFERRED AGE (GRAY COLUMN) IS EITHER THE $^{207}Pb/^{206}Pb$ OR THE $^{238}U/^{206}Pb$ AGE WITH THE LOWEST DEGREE OF DISCORDANCE RELATIVE TO THE CONCORDIA LINE (*i.e.*, 1σ error).

Sample and spot #	U [ppm]	Th/U	$^{238}U/^{206}Pb$	± 1σ [%]	$^{207}Pb/^{206}Pb$	± 1σ [%]	$^{206}Pb/^{238}U$ Age	± 1σ [Ma]	$^{207}Pb/^{206}Pb$	± 1σ [Ma]	Preferred Age	± 1σ [Ma]
PR-11-123-1	100	1.3	0.0525	2.1	18.8228	7.6	330.0	6.9	334.2	171.4	330.0	6.9
PR-11-123-1R	14	2.6	0.0552	8.8	22.7329	63.6	346.4	29.8	-111.3	1738.5	346.4	29.8
PR-11-123-2C	227	1.0	0.0544	1.1	18.9113	2.7	341.6	3.7	323.6	61.3	341.6	3.7
PR-11-123-3C	579	2.6	0.0548	1.6	18.6625	1.3	343.7	5.5	353.6	29.1	343.7	5.5
PR-11-123-3R	262	4.0	0.0550	2.2	18.4121	2.0	345.2	7.4	384.0	45.4	345.2	7.4
PR-11-123-4C	333	1.1	0.0502	1.6	19.8328	3.2	315.8	4.8	214.5	74.0	315.8	4.8
PR-11-123-4R	576	1.6	0.0499	2.2	19.0104	1.6	313.9	6.6	311.7	36.3	313.9	6.6
PR-11-123-5C	168	3.7	0.0523	1.3	19.5149	3.9	328.5	4.1	251.8	89.5	328.5	4.1
PR-11-123-5R	221	2.6	0.0533	2.0	19.0126	2.0	335.0	6.5	311.4	45.3	335.0	6.5
PR-11-123-6C	275	0.5	0.0094	3.4	20.9155	9.0	60.4	2.1	89.9	214.8	60.4	2.1
PR-11-123-6R	274	0.5	0.0100	5.9	18.8785	12.8	63.8	3.8	327.5	291.7	63.8	3.8
PR-11-123-7C	114	1.2	0.0540	2.1	19.3769	4.7	339.0	6.8	268.1	107.0	339.0	6.8
PR-11-123-7R	122	1.9	0.0575	3.3	19.4626	2.3	360.6	11.7	258.0	53.5	360.6	11.7
PR-11-123-8C	66	1.4	0.0565	3.5	19.2067	9.4	354.5	12.1	288.3	216.0	354.5	12.1
PR-11-123-8R	92	1.7	0.0546	4.3	19.4018	5.7	342.8	14.4	265.1	130.4	342.8	14.4
PR-11-123-9C	93	1.2	0.0480	1.6	19.4508	6.6	302.2	4.9	259.3	152.1	302.2	4.9
PR-11-123-9R	217	0.9	0.0486	1.5	19.3005	3.0	305.6	4.4	277.1	68.4	305.6	4.4
PR-11-123-10C	101	1.2	0.0540	1.8	18.8729	6.5	339.3	6.0	328.2	147.6	339.3	6.0
PR-11-123-10R	97	1.5	0.0544	1.6	19.6292	7.0	341.6	5.2	238.3	161.0	341.6	5.2
PR-11-123-11C	239	1.6	0.0536	1.8	18.9899	3.4	336.7	5.9	314.2	76.6	336.7	5.9
PR-11-123-11R	239	2.2	0.0543	1.7	18.7253	3.2	340.8	5.8	346.0	73.4	340.8	5.8
PR-11-123-12C	516	5.2	0.0529	2.1	18.9022	1.4	332.3	6.8	324.7	32.0	332.3	6.8
PR-11-123-12R	426	5.0	0.0550	1.6	19.0728	1.8	344.9	5.5	304.3	40.1	344.9	5.5
PR-11-123-13C	116	2.1	0.0480	2.1	18.3738	8.5	301.9	6.3	388.7	190.0	301.9	6.3
PR-11-123-13R	261	4.2	0.0483	4.2	19.1231	2.6	304.0	12.4	298.2	58.5	304.0	12.4
PR-11-123-14C	121	2.9	0.0538	2.2	19.0948	2.2	337.6	7.2	301.6	50.3	337.6	7.2
PR-11-123-14R	151	6.8	0.0521	6.6	18.7119	6.2	327.6	21.0	347.6	140.1	327.6	21.0
PR-11-123-15C	103	2.6	0.0536	4.5	20.1394	7.8	336.6	14.7	178.8	182.7	336.6	14.7

Table 3 continued.

Sample and spot #	U [ppm]	Th/U	$^{238}U/^{206}Pb$	± 1σ [%]	$^{207}Pb/^{206}Pb$	± 1σ [%]	$^{206}Pb/^{238}U$ Age	± 1σ [Ma]	$^{207}Pb/^{206}Pb$	± 1σ [Ma]	Preferred Age	± 1σ [Ma]
PR-11-123-15R	131	4.4	0.0554	6.2	18.6750	6.7	347.8	20.8	352.1	151.2	347.8	20.8
PR-11-123-16C	63	1.2	0.0481	2.7	19.1422	10.4	302.6	7.9	295.9	238.6	302.6	7.9
PR-11-123-16R	70	1.2	0.0471	3.7	19.3692	12.5	297.0	10.8	269.0	288.0	297.0	10.8
PR-11-123-17C	390	1.5	0.0093	3.7	24.3699	11.9	60.0	2.2	-285.4	303.3	60.0	2.2
PR-11-123-17R	406	2.6	0.0093	2.2	22.5507	17.8	59.4	1.3	-91.5	439.6	59.4	1.3
PR-11-123-18C	148	2.0	0.0533	2.1	19.3189	5.0	334.8	7.0	274.9	114.3	334.8	7.0
PR-11-123-18R	155	2.5	0.0526	2.2	18.3669	4.5	330.3	7.2	389.5	100.6	330.3	7.2
PR-11-123-19C	98	1.5	0.0539	1.6	19.3016	7.9	338.5	5.3	277.0	180.9	338.5	5.3
PR-11-123-19R	152	1.2	0.0544	1.2	19.0097	4.0	341.2	3.9	311.8	91.3	341.2	3.9
PR-11-123-20R	403	10.5	0.0266	4.2	18.6743	4.1	169.0	7.0	352.1	92.3	169.0	7.0
PR-11-123-21C	124	2.8	0.0522	3.9	19.4985	5.0	327.7	12.4	253.7	114.3	327.7	12.4
PR-11-123-21R	228	3.8	0.0483	3.7	19.0286	3.0	304.1	10.9	309.5	67.8	304.1	10.9
PR-11-123-22C	111	1.4	0.2683	15.1	9.9677	6.5	1,532.1	205.9	1,630.1	121.5	1,630.1	121.5
PR-11-123-22R	691	10.2	0.1654	5.8	12.6634	0.7	986.9	52.9	1,171.3	13.2	1,171.3	13.2
PR-11-123-23C	752	1.2	0.0535	1.0	18.8061	1.8	336.1	3.3	336.3	40.1	336.1	3.3
PR-11-123-23R	840	1.3	0.0531	1.4	18.4368	3.9	333.8	4.6	381.0	88.1	333.8	4.6
PR-11-123-24C	283	8.7	0.0549	1.0	18.6840	3.2	344.5	3.5	351.0	73.2	344.5	3.5
PR-11-123-24R	294	9.4	0.0544	3.8	18.6638	4.4	341.4	12.8	353.4	98.8	341.4	12.8
PR-11-123-25C	188	3.6	0.1518	7.8	13.5682	2.1	911.0	66.5	1,033.3	41.9	1,033.3	41.9
PR-11-123-25R	283	8.9	0.0585	3.7	18.2815	1.9	366.7	13.2	400.0	43.4	366.7	13.2
PR-11-123-26C	475	7.0	0.0552	1.6	18.9680	1.7	346.3	5.3	316.8	38.2	346.3	5.3
PR-11-123-26R	377	2.8	0.0544	1.3	18.9474	1.7	341.5	4.3	319.2	37.7	341.5	4.3
DRH-TF11-04-01	743	1.3	0.0264	1.9	19.9867	2.5	167.9	3.1	196.6	58.4	167.9	3.1
DRH-TF11-04-02	118	1.4	0.0251	7.5	26.0025	35.3	159.9	11.9	-453.5	954.2	159.9	11.9
DRH-TF11-04-03	231	0.9	0.0230	1.8	20.6445	11.0	146.4	2.6	120.7	260.8	146.4	2.6
DRH-TF11-04-04	120	1.3	0.0247	4.5	23.9583	15.7	157.4	7.0	-242.2	398.5	157.4	7.0
DRH-TF11-04-05	133	1.2	0.0253	5.7	24.0754	20.8	161.0	9.0	-254.6	531.7	161.0	9.0

Table 3 continued.

Sample and spot #	U [ppm]	Th/U	$^{238}U/^{206}Pb$	± 1σ [%]	$^{207}Pb/^{206}Pb$	± 1σ [%]	$^{206}Pb/^{238}U$ Age	± 1σ [Ma]	$^{207}Pb/^{206}Pb$	± 1σ [Ma]	Preferred Age	± 1σ [Ma]
DRH-TF11-04-06	107	1.2	0.0241	4.0	23.2492	43.5	153.7	6.1	-166.9	1130.7	153.7	6.1
DRH-TF11-04-07	74	1.5	0.0252	5.2	17.7545	19.0	160.5	8.2	465.1	424.9	160.5	8.2
DRH-TF11-04-08	35	1.6	0.0246	11.8	0.9092	4,319.9	156.4	18.2	0.0	887.6	156.4	18.2
DRH-TF11-04-09	25	2.2	0.0238	14.1	23.7811	73.6	151.4	21.0	-223.5	2,159.6	151.4	21.0
DRH-TF11-04-10	60	1.9	0.0240	6.5	20.2290	35.1	153.1	9.8	168.4	843.2	153.1	9.8
DRH-TF11-04-11	58	2.1	0.0234	9.1	22.6514	33.5	149.3	13.5	-102.4	844.2	149.3	13.5
DRH-TF11-04-12	582	1.0	0.0250	1.1	20.7168	4.0	159.4	1.8	112.5	95.0	159.4	1.8
DRH-TF11-04-13	81	1.3	0.0236	6.4	28.4484	32.3	150.5	9.5	-696.6	915.5	150.5	9.5
DRH-TF11-04-14	86	1.3	0.0240	5.9	17.5954	23.4	152.8	8.9	485.1	523.3	152.8	8.9
DRH-TF11-04-15	64	1.5	0.0238	7.7	24.9313	35.2	151.3	11.5	-343.8	932.5	151.3	11.5
DRH-TF11-04-16	42	2.1	0.0235	13.4	17.6725	84.0	150.0	19.9	475.4	2,402.4	150.0	19.9
DRH-TF11-04-17	53	2.0	0.0223	11.8	5.7286	811.3	142.1	16.6	2601.9	1,414.8	142.1	16.6
DRH-TF11-04-18	71	1.3	0.0242	6.4	28.7721	44.5	153.9	9.7	-728.1	1,296.9	153.9	9.7
DRH-TF11-04-19	113	1.1	0.0237	4.4	19.6255	19.1	151.0	6.6	238.7	443.2	151.0	6.6
DRH-TF11-04-20	109	1.1	0.0237	6.5	24.8673	35.5	151.1	9.7	-337.2	939.6	151.1	9.7
DRH-TF11-04-21	80	1.5	0.0241	5.3	25.8012	29.2	153.4	8.0	-433.1	781.5	153.4	8.0
DRH-TF11-04-22	50	1.7	0.0244	10.6	17.3503	40.2	155.2	16.3	515.9	919.0	155.2	16.3
DRH-TF11-04-23	64	2.3	0.0235	4.9	25.9946	50.2	149.6	7.3	-452.7	1,399.6	149.6	7.3
DRH-TF11-04-24	82	1.4	0.0259	7.4	21.2937	18.3	165.0	12.1	47.3	441.4	165.0	12.1
DRH-TF11-04-26	55	1.6	0.0238	7.6	20.9524	36.4	151.7	11.4	85.8	890.2	151.7	11.4
DRH-TF11-04-27	85	1.9	0.0241	4.9	25.1299	43.6	153.4	7.5	-364.3	1,176.5	153.4	7.5
DRH-TF11-04-28	57	1.9	0.0235	8.9	21.4463	85.2	149.9	13.2	30.2	2,641.5	149.9	13.2
DRH-TF11-04-30	93	1.5	0.0234	8.2	22.3183	29.5	149.4	12.2	-66.2	734.3	149.4	12.2
DRH-TF11-04-31	71	1.5	0.0243	5.2	19.3555	28.2	154.5	7.9	270.6	658.2	154.5	7.9
DRH-TF11-04-32	89	1.6	0.0234	5.6	34.4345	36.5	149.2	8.2	-1259.9	1,177.7	149.2	8.2
DRH-TF11-04-33	37	1.7	0.0244	11.5	7.3632	171.0	155.3	17.6	2,174.4	100.0	155.3	17.6
DRH-TF11-04-34	55	2.7	0.0234	8.2	19.1891	50.2	149.2	12.1	290.3	1,220.9	149.2	12.1
DRH-TF11-04-35	76	1.3	0.0249	4.4	20.6699	39.5	158.3	6.9	117.9	966.5	158.3	6.9
DRH-TF11-04-36	50	1.8	0.0239	8.2	-4.5169	610.1	152.4	12.4	0.0	72.2	152.4	12.4

Table 3 continued.

Sample and spot #	U [ppm]	Th/U	$^{238}U/^{206}Pb$	± 1σ [%]	$^{207}Pb/^{206}Pb$	± 1σ [%]	$^{206}Pb/^{238}U$ Age	± 1σ [Ma]	$^{207}Pb/^{206}Pb$	± 1σ [Ma]	Preferred Age	± 1σ [Ma]
DRH-TF11-04-37	45	1.6	0.0249	10.8	32.0652	143.0	158.4	16.9	-1041.3	0.0	158.4	16.9
DRH-TF11-04-38	34	2.0	0.0244	11.9	18.0705	56.6	155.6	18.3	425.9	1372.6	155.6	18.3
DRH-TF11-04-39	48	2.1	0.0241	12.2	-6.0070	639.7	153.3	18.5	0.0	537.0	153.3	18.5
DRH-TF11-04-40	89	1.2	0.0240	4.8	23.8860	22.9	152.8	7.2	-234.6	584.6	152.8	7.2
DRH-TF11-04-41	551	0.9	0.0258	1.0	19.9390	5.8	163.9	1.7	202.1	134.8	163.9	1.7
DRH-TF11-04-42	165	1.3	0.0236	4.5	23.4158	16.9	150.6	6.6	-184.7	425.4	150.6	6.6
DRH-TF11-04-43	142	1.3	0.0241	4.5	21.7155	24.4	153.7	6.9	0.3	595.0	153.7	6.9
DRH-TF11-04-44	96	1.3	0.0241	2.2	25.0870	29.9	153.3	3.3	-359.9	788.0	153.3	3.3
DRH-TF11-04-45	46	1.7	0.0239	6.4	9.4789	222.2	152.3	9.7	1723.0	448.9	152.3	9.7
DRH-TF11-04-46	148	1.2	0.0239	3.2	22.8034	20.3	152.1	4.8	-118.9	505.8	152.1	4.8
DRH-TF11-04-48	88	1.4	0.0243	4.5	22.8172	40.1	154.7	6.9	-120.4	1,024.8	154.7	6.9
DRH-TF11-04-50	66	1.9	0.0231	9.2	28.0171	162.0	147.3	13.4	-654.4	0.0	147.3	13.4
DRH-TF11-04-51	57	2.0	0.0237	8.8	18.4251	31.3	151.2	13.1	382.4	720.2	151.2	13.1
DRH-TF11-04-52	59	1.8	0.0247	11.3	24.6712	59.6	157.6	17.5	-316.9	1,668.5	157.6	17.5
DRH-TF11-04-53	593	1.9	0.0257	1.2	20.1049	3.2	163.5	1.9	182.8	75.0	163.5	1.9
DRH-TF11-04-54	77	1.2	0.0239	7.2	27.6237	41.7	152.3	10.9	-615.7	1,180.8	152.3	10.9
DRH-TF11-04-56	47	1.9	0.0229	11.5	20.7883	37.6	145.8	16.5	104.4	917.8	145.8	16.5
DRH-TF11-04-57	92	1.2	0.0232	10.1	37.8593	46.7	147.7	14.8	-1568.8	1,648.9	147.7	14.8
DRH-TF11-04-58	68	1.2	0.0235	8.8	28.5826	67.6	150.0	13.0	-709.7	2,107.7	150.0	13.0
DRH-TF11-04-59	47	1.7	0.0238	9.2	25.2388	55.1	151.6	13.7	-375.5	1,534.2	151.6	13.7
DRH-TF11-04-60	98	1.4	0.0230	5.7	23.0943	25.4	146.9	8.3	-150.3	639.8	146.9	8.3
DRH-TF11-04-61	754	1.4	0.0253	1.7	19.9679	2.8	161.2	2.7	198.7	66.1	161.2	2.7
DRH-TF11-04-62	54	1.3	0.0240	10.0	21.7219	42.0	153.1	15.1	-0.4	1,055.2	153.1	15.1
DRH-TF11-04-63	46	2.1	0.0233	12.1	35.4644	291.1	148.6	17.8	-1353.5	0.0	148.6	17.8
DRH-TF11-04-64	68	1.6	0.0248	5.6	19.9352	17.7	158.2	8.7	202.5	412.6	158.2	8.7
DRH-TF11-04-65	47	1.7	0.0233	11.8	24.8110	41.3	148.6	17.3	-331.4	1,103.4	148.6	17.3
DRH-TF11-04-66	116	1.3	0.0248	6.8	17.2881	18.9	158.1	10.6	523.8	418.5	158.1	10.6
DRH-TF11-04-67	79	1.8	0.0245	4.7	29.3404	39.1	156.1	7.2	-783.1	1,141.0	156.1	7.2
DRH-TF11-04-68	56	1.1	0.0236	9.3	22.8353	45.9	150.7	13.8	-122.4	1,188.8	150.7	13.8

Table 3 continued.

Sample and spot #	U [ppm]	Th/U	$^{238}U/^{206}Pb$	± 1σ [%]	$^{207}Pb/^{206}Pb$	± 1σ [%]	$^{206}Pb/^{238}U$ Age	± 1σ [Ma]	$^{207}Pb/^{206}Pb$	± 1σ [Ma]	Preferred Age	± 1σ [Ma]
DRH-TF11-04-69	73	1.2	0.0243	5.7	24.4583	38.0	154.7	8.7	-294.7	1001.3	154.7	8.7
DRH-TF11-04-70	74	1.1	0.0237	9.2	27.2725	38.9	150.8	13.8	-580.9	1086.2	150.8	13.8
DRH-TF11-04-71	49	2.2	0.0232	12.2	-1.4331	1957.6	148.1	17.9	0.0	258.0	148.1	17.9
DRH-TF11-04-72	174	1.7	0.0253	2.2	19.0882	20.5	161.1	3.5	302.4	472.5	161.1	3.5
DRH-TF11-04-73	86	1.3	0.0241	4.8	20.1474	26.5	153.5	7.3	177.9	627.7	153.5	7.3
DRH-TF11-04-74	98	1.2	0.0243	5.1	23.0649	21.4	154.5	7.7	-147.1	534.7	154.5	7.7
DRH-TF11-04-75	76	1.6	0.0236	5.3	26.0206	28.1	150.4	7.9	-455.4	752.1	150.4	7.9
DRH-TF11-04-76	62	1.7	0.0247	6.9	23.5920	35.5	157.1	10.7	-203.4	914.3	157.1	10.7
DRH-TF11-04-77	62	1.6	0.0244	8.9	16.4401	51.8	155.6	13.6	633.1	1,194.7	155.6	13.6
DRH-TF11-04-78	49	1.6	0.0244	5.9	31.1980	62.9	155.3	9.0	-960.0	2,025.8	155.3	9.0
DRH-TF11-04-79	67	1.6	0.0243	7.4	22.4175	52.3	154.8	11.3	-77.0	1,365.5	154.8	11.3
DRH-TF11-04-81	46	1.0	0.0241	11.7	17.5381	61.5	153.5	17.7	492.3	1,503.5	153.5	17.7
DRH-TF11-04-82	62	1.2	0.0285	9.2	23.4923	24.4	180.8	16.5	-192.8	617.9	180.8	16.5
DRH-TF11-04-83	86	0.9	0.0250	3.8	22.1112	23.7	159.2	5.9	-43.4	584.0	159.2	5.9
DRH-TF11-04-84	44	1.7	0.0241	7.5	24.8768	51.3	153.5	11.4	-338.2	1,405.0	153.5	11.4
DRH-TF11-04-85	57	1.4	0.0249	7.0	35.7139	42.0	158.6	11.0	-1,376.1	1,407.2	158.6	11.0
DRH-TF11-04-86	135	1.1	0.0238	2.1	22.3357	13.6	151.7	3.2	-68.1	334.5	151.7	3.2
DRH-TF11-04-88	141	1.3	0.0231	4.2	22.4801	13.5	147.2	6.1	-83.8	332.0	147.2	6.1
DRH-TF11-04-91	62	1.4	0.0244	6.6	27.6614	52.7	155.1	10.1	-619.4	1,531.2	155.1	10.1
DRH-TF11-04-92	40	1.5	0.0255	11.1	37.7432	68.2	162.2	17.7	-1,558.4	636.8	162.2	17.7
DRH-TF11-04-93	66	2.0	0.0244	6.9	38.2223	60.2	155.6	10.5	-1,601.1	398.0	155.6	10.5
DRH-TF11-04-94	97	1.7	0.0232	8.3	23.1940	30.4	147.6	12.1	-161.0	770.4	147.6	12.1
DRH-TF11-04-95	51	1.9	0.0239	6.3	26.0615	55.4	152.1	9.5	-459.5	1,570.3	152.1	9.5
DRH-TF11-04-96	29	1.8	0.0244	11.0	11.7195	50.4	155.1	16.9	1,323.0	1,048.4	155.1	16.9
DRH-TF11-04-97	84	1.6	0.0241	4.9	19.2723	24.5	153.4	7.5	280.5	567.6	153.4	7.5
DRH-TF11-04-98	68	1.6	0.0254	7.9	21.0165	26.4	161.9	12.6	78.5	635.6	161.9	12.6
DRH-TF11-04-100	38	2.0	0.0242	6.0	12.3622	30.2	154.0	9.1	1218.8	607.9	154.0	9.1
DRH-TF11-04-R33	82	2.3	0.0665	1.7	19.5027	9.3	414.9	7.0	253.2	214.5	414.9	7.0
DRH-TF11-04-R33	108	1.4	0.0666	1.9	17.8182	11.6	415.8	7.5	457.2	257.4	415.8	7.5

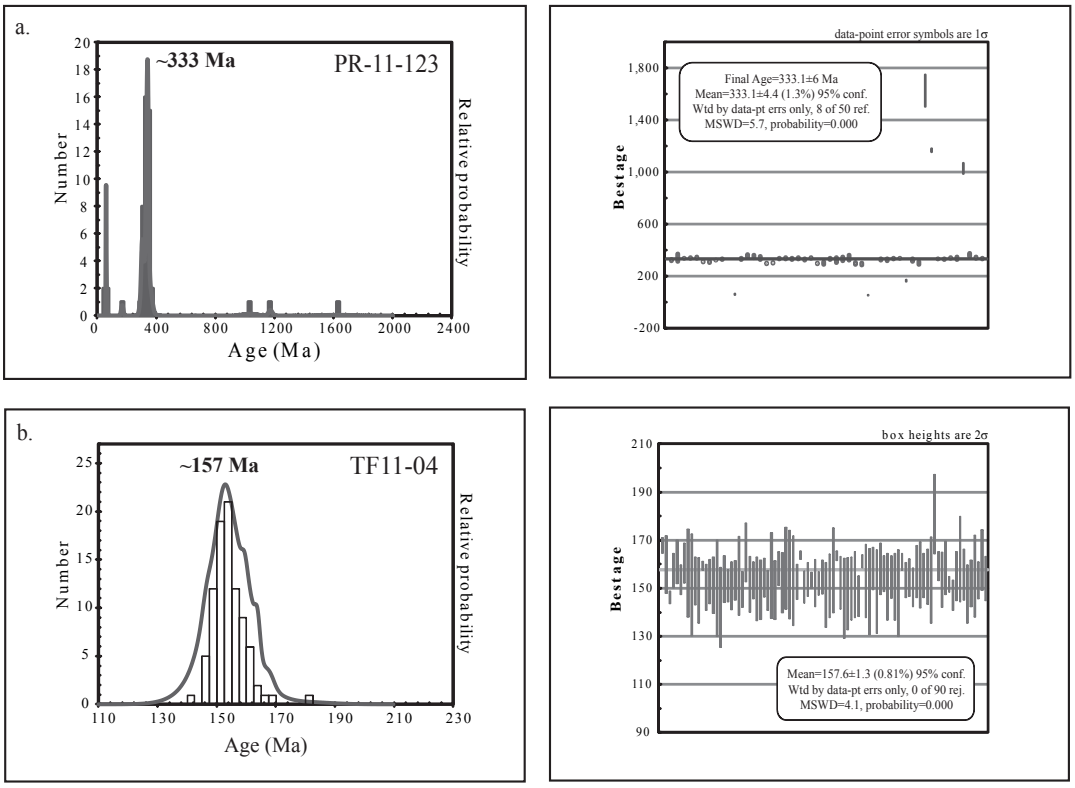

FIG. 9. Probability density plots for the preferred U-Pb ages of the two selected samples **a.** sample PR-11-123 is a granitic clast sampled from a breccia at the Río Volcan section; **b.** sample TF11-04 is a red sandstone from the top of the sedimentary sequence at the Termas del Flaco section.

del Flaco and Vaca Muerta formations. This would indicate that either the Tithonian age assigned to the fossiliferous content of the overlynig units or the age assumed for the Kimmeridgian/Tithonian and Jurassic/Cretaceous boundaries are wrong. Whatever is the reason for the disagreement between the stratigraphic *versus* absolute ages of the Río Damas-Tordillo Formation, the results presented in this work are consistent with other maximum depositional ages obtained in sedimentary rocks of the same unit in the Río Volcán area, and in the southern part of the Neuquén basin, that have extended the age range of the Río Damas-Tordillo Formation into the Tithonian and, as in the study region, even into the earliest Cretaceous (Aguirre *et al.*, 2009; Cucchi *et al*., 2005; Leanza and Hugo, 1997; Naipauer *et al*., 2012, 2014). Therefore, the events of continental clastic desposition in the western and southern margin of the Neuquén basin would have been continuous beyond the Kimmeridgian/Tithonian and even the Jurassic/Cretaceous boundary, practically overlaping the maximum age assigned to the overlaying marine deposits of the Vaca Muerta (early late Tithonian), and lower Lo Valdés (Tithonian) and Termas del Flaco (Late Tithonian) formations (Biro-Bagoczky, 1964, 1980; Charrier, 1981; Hallam *et al*., 1986; Klohn, 1960; Leanza, 1981; Riccardi, 2008a, b; Thiele, 1980). The volcanic intercalation of basaltic andesitic lavas and breccias of the Río Damas-Tordillo Formation should have been emplaced in a restricted time span. Volcanic activity was probably facilitated by the presence of extensional structures related to the formation of the back-arc basin (Charrier *et al*., 2007).

The main peak of 157.6±1.3 Ma observed in the zircon population of sample TF11-04, with zircons as old as ~170 Ma, is consistent with the reported ages of plutonic bodies and dikes cropping out in the Coastal Cordillera of central Chile (Creixell *et al*., 2006; Gana and Tosdal, 1996; Godoy and Loske, 1988;

Hervé *et al*., 1988; Parada *et al*., 1999) suggesting that this area would have been the main source of sediments feeding the back-arc basin during Upper Jurassic. This implies that an important part of the Jurassic arc domain was exhumed and eroded in Oxfordian and Tithonian times, exposing the epizonal intrusives of Middle Jurassic age, and probably the upper part of the Horqueta Formation.

The age of 333.1±4.4 Ma obtained in the granitic fragment located at the top of the Río Volcán section; represents the first reported evidence for Carboniferous sources for sediments of the Río Damas-Tordillo Formation at this latitude. Recent studies of the Jurassic sequences in the southern end of the Neuquén basin have shown an important component of Paleozoic zircons in clastic sediments of Tordillo and Quebrada del Sapo formations, being interpreted as the result of erosion of the exposed basement in the Huincul High (Naipauer *et al*., 2012). However, this topographic relief was located too far in the south (39°S) to be considered as a likely source of the sediments that accumulated at the present-day 33-35°S latitudes. Sediments of late Paleozoic age have also been identified in red clastic sequences of Kimmeridgian/Tithonian age in northern Chile, and their likely sources attributed to numerous Carboniferous to Permian intrusions that crop out in the Principal Cordillera (28-29°S; Oliveros *et al*., 2012). At the latitude of the present study, no Paleozoic plutonic rocks older than 320 Ma have been reported in the Chilean territory (Deckart *et al*., 2014). Given the large size of the granitic clasts, their source must have been an unexposed extension of Carboniferous granitoid located near the Chile-Argentina border, rather than the present-day nearest outcrops of Paleozoic granitoids in the Coastal Cordillera between 33° and 38°S.

An important feature to take into account for the Río Damas-Tordillo Formation is the rough variations in the architecture of the stratigraphic sections in the different studied locations. As we show in figure 5, major variations in the thickness and disposition of the sedimentary and volcanic deposits can be observed in studied areas. In the Río Volcán section, the Río Damas-Tordillo Formation is composed of a basal level of mostly volcanic rocks, overlied by a thick sequence of continental clastic sediments, while in the Termas del Flaco area the volcanic rocks overlie the clastic sedimentary deposits. Considering the important amount of large volcanic clasts of the same composition observed in the base of the sequence, we interpret these variations as the result of a mayor tectonic cannibalism in the northern area, related to a more active faulting.

6.2. Constrains on the magma sources of the Río Damas-Tordillo volcanism

The volcanic rocks of the Río Damas-Tordillo Formation are characterized by an enrichment in LILE compared to HFSE, negative slopes in the REE diagrams, marked Nb-Ta negative and positive Ce anomalies. Such characteristics are considered as representative of subduction-related magmas (Pearce, 1982), and are typical of calc-alkaline magmatism globally (Fig. 10). In both the trace elements and REE diagrams, samples show sub-parallel trends, suggesting that they have a co-genetic origin and are the result of various degrees of differentiation from a common source.

The Mg# and the MgO contents of the analyzed samples (Table 1) indicate that no primitive magmas were analyzed and suggest previous olivine and clinopyroxene fractionation. Nb/Zr ratios (Fig. 11a) are indicative of mantle depletion as they are not influenced by fluid enrichment or fractional crystallization; Nb/Zr ratios and multielement diagrams of the analyzed samples have a narrow range similar

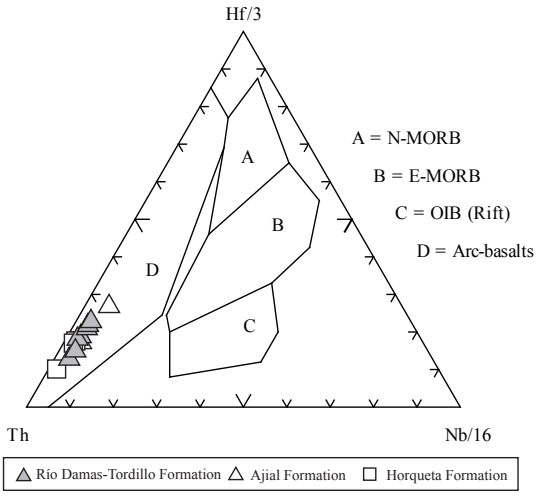

FIG. 10. Tectonic setting discrimination diagram (Cabanis and Lecolle, 1989) for volcanic (basic- intermediate) rocks in the studied area. Ajial and Horqueta Formation samples in the Coastal Cordillera in Central Chile after Vergara *et al.,* 1995.

to the normal mid-ocean ridge basalts (N-MORB) composition, and indicate either slight depletion or enrichment relative to N-MORB. Low $(La/Yb)_N$ ratios (4-5.4) or flat REE patterns are interpreted as the result of partial melting of a depleted mantle source. $Yb_N>10$ excludes the possibility of the garnet as a residual phase in the source of the Río Damas-Tordillo magmas.

The high abundances of Ba, K and Sr relative to HFSE, such as Nb and Ta, would favor the hypothesis of fluid enrichment in the slab/mantle boundary of a subduction zone (Peate *et al*., 1997). The Th/La *versus* Sm/La diagram can be used to trace the addition of sediments to the mantle wedge beneath the arc (Plank, 2005), or contamination of the magmas by forearc subduction erosion or during interaction with the crust (Hildreth and Moorbath, 1988; Stern, 1991, 2011). In figure 11a, the rocks of the Río Damas-Tordillo Formation plot slightly aligned to the sediment/crust contamination vector, suggesting that this process would control the generation of the parental magmas, as it is in the case of the Jurassic Horqueta and Ajial Formations volcanism. However, given the small number of samples analyzed for this study the last observation should be taken with caution.

High variability in Ba and Sr contents probably reflects feldspar alteration, which is consistent with the pervasive sericite replacement observed in the plagioclase phenocrsyts. Low abundances of Zr, V, Y and REE in sample MO208-385 could be the result of the intense alteration of the rock.

The Nd-Sr isotopic composition of the Río Damas-Tordillo Formation lavas is in the range of the Jurassic volcanic and plutonic rocks (arc magmatism) cropping out in the Coastal Cordillera in northern and central Chile (Kramer *et al*., 2004; Lucassen *et al*., 2006; Rossel *et al*., 2013;Vergara *et al*., 1995). Therefore, it is possible to infer a depleted mantle source for the magmas of the Río Damas-Tordillo Formation, similar to that of the Jurassic arc magmatism and some back-arc volcanics like the Quebrada Vicuñita Beds, at 26-28°S, but different from the sources of the other back-arc units of northern Chile (Rossel *et al*., 2013).

On the other hand, Pb isotopes show a large dispersion between the Jurassic Arc field and the average Paleozoic Crust composition (Fig. 8b). This suggests different degrees of crustal assimilation, which is more evident in this system because of the small amounts of radiogenic Pb in the mantle and high Pb in the crust. The compositional variations in the Pb isotopes is in part also due to the pervasive alteration of the studied rocks as well.

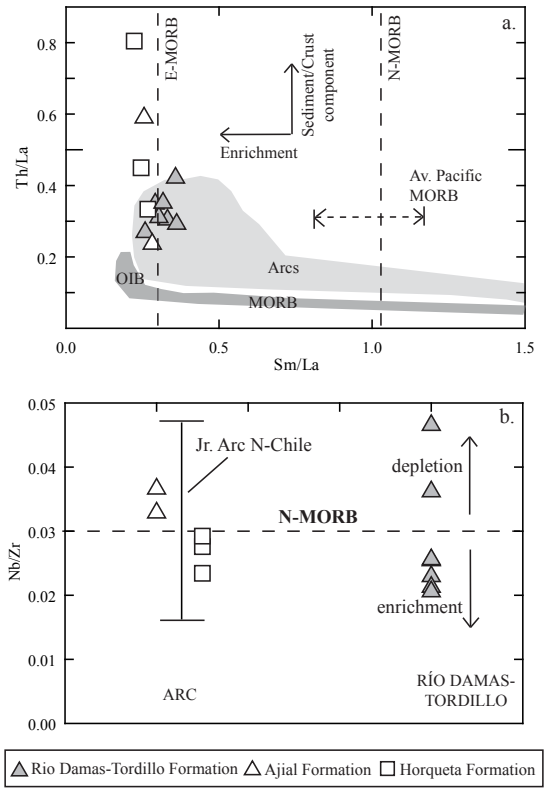

FIG. 11. **a.** Th/La *versus* Sm/La diagram. Arcs, OIB and MORB fields, enrichment and sediment component vectors and Average Sm/La values for normal, enriched and Pacific MORB (dotted lines: N.MORB, E-MORB, Pacific MORB) are after Plank (2005); **b.** Nb/Zr ratios, N-MORB value in dotted line is after Sun and McDonough (1989). Data from Ajial and Horqueta Formations in the Coastal Cordillera of Central Chile are after Vergara *et al.* (1995).

In order to better constrain the source of the Río Damas-Tordillo lavas and the Jurassic arc rocks of central Chile, Equilibrated Melting, Assimilation and Fractional Crystallization (AFC) and mixing forward modeling were performed using our elemental data (Fig. 12). The results show that it is possible to achieve the compositional features of the most primitive samples of the arc and the Río Damas-Tordillo Formation by 15% melting of a mixture of 80% Depleted Mantle (DM) and 20% Primitive Mantle (PM), and subsequent fractionation of olivine with minor amounts (<10%) of assimilation of lower crust. To achieve the composition of the more evolved arc

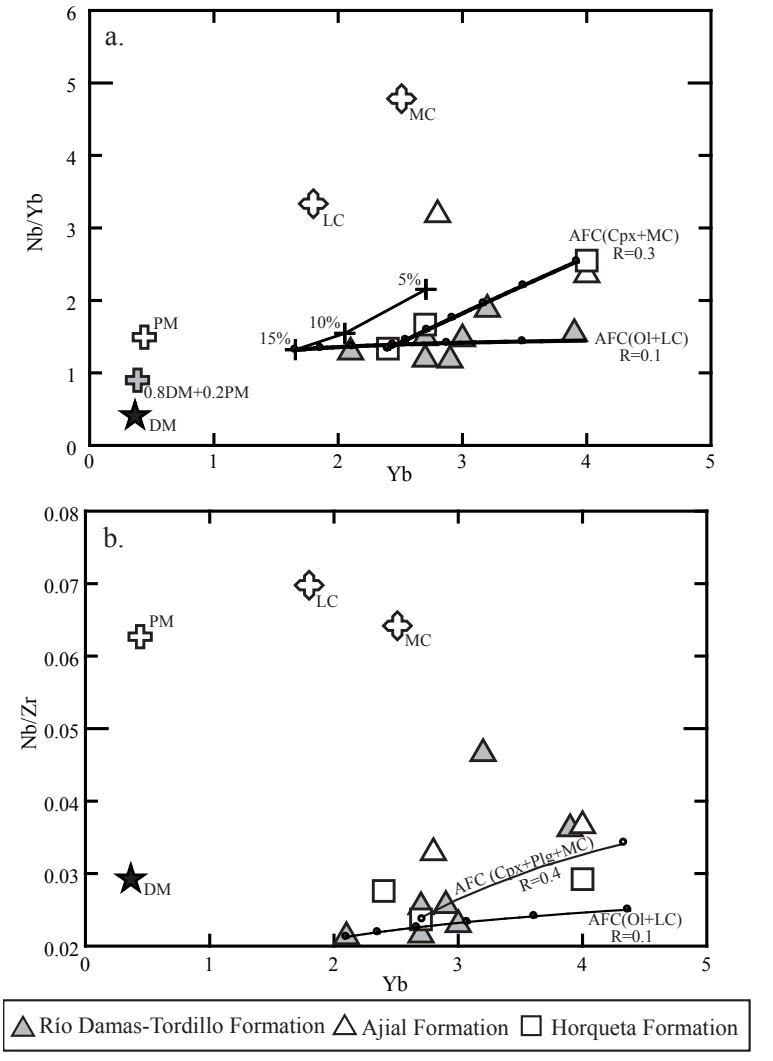

FIG. 12. **a.** Nb/Yb *versus* Yb and **b.** Nb/Zr *versus* Yb diagrams for Jurassic arc and back-arc volcanic rocks in central Chile. Trajectories with crosses represent Equilibrated Melting in steps of 5%. Lines with circles represent AFC process after DePaolo (1981), the 'r' factor in the AFC equation is shown. Steps in crystallization model are 10%. Starting values in a) is the modeled concentration of Nb, Zr and Yb after 15% of melting of a mixture of 80% of DM and 20% of PM. Starting values in b) are the measured concentrations of Nb, Zr and Yb in the less differentiated sampleof the Río Damas Fm. (MO208-385) and in sample Mel22 of the Horqueta Fm. (Vergara *et al.,* 1995). **LC:** Lower Continental Crust and **MC:** Middle Continental Crust, after Rudnick and Gao (2003).Data from Ajial and Horqueta Formations in the Coastal Cordillera ofcentral Chile after Vergara *et al.* (1995).

samples, the assimilation of significant amounts of middle continental crust, along with progressive fractionation of clinopyroxene and plagioclase is required. This is consistent with the observed Eu anomalies and the high Sr isotope ratios reported by Vergara *et al*. (1995).

Unlike in northern Chile (26°-30°S), where geochemical variations between the Jurassic arc and back-arc magmatism are clearly observed (Rossel *et al*., 2013), it is not possible to differentiate the sources and processes involved in the generation of the arc magmatism in central Chile and the lavas of the Río Damas-Tordillo Formation based only in the elemental and isotopic composition of these rocks. The volcanism of the Río Damas-Tordillo Formation could therefore represent arc activity.

6.3. A tectonic framework for the Río Damas-Tordillo Formation

Taking into account the geochemistry, petrology and probably age of the Río Damas-Tordillo lavas according to the new dates here suplied and its stratigraphic location, we propose the following evolutionary model for the latest Jurassic deposits in central Chile and Argentina between 32°5' and 35°S (Fig. 13).

During the Lower and Middle Jurassic the transtensional/extensional regime of subduction in the Andean margin (Charrier *et al*., 2007; Grocott and Taylor, 2002; Mpodozis and Ramos, 2008; Scheuber and González, 1999) resulted in a paleogeographic configuration characterized by the development of a voluminous volcanic arc that was mostly submerged considering the numerous intercalations of marine deposits between the lavas of the Ajial Formation in the Coastal Cordillera (Charrier *et al*., 2007; Vergara *et al*., 1995). The inferred paleogeography suggests that a connection existed between the Pacific Ocean and the Neuquén basin to the east (Legarreta and Uliana, 1999; Howell *et al*., 2005).

Between the Middle and Upper Jurassic, the change to transpressional regime has been proposed in northern and central Chile, probably as the result of an increased coupling between the two plates (Creixell *et al*., 2011; Ring *et al*., 2012; Scheubert and González, 1999). This change, in addition to the accumulation of volcanic material, could be responsible of the progressive emersion of the arc and probably the forearc domain, and subsequent disconnection of the back-arc with the Pacific Ocean during Kimmeridgian and Tithonian times (Klohn, 1960; Legarreta *et al*., 1999; Mescua, 2011; Thiele, 1980), leading to continental sedimentation in both domains, as recorded by Horqueta Formation (arc) and Río Damas-Tordillo Formation (back-arc).

During the Kimmeridgian and Tithonian, the back-arc at the studied latitudes show evidences for extensional conditions, with sedimentation controlled by normal faulting (Cegarra and Ramos, 1996; Charrier *et al*., 2007; Giambiagi *et al*., 2003; Mescua *et al*., 2008; Pángaro *et al*., 1996). The plate coupling probably concentrated the deformation in the arc domain due to thermal softening, avoiding the development of compressive or transpresive structures in back-arc domain.

The regional long-term extension since the beginning of the Mesozoic (Legarreta and Uliana, 1999) led to a progressive thinning of crust (Charrier *et al*., 2007; Mpodozis and Ramos, 2008), which together with the presence of active normal faults, likely favored the rapid ascent of important volumes of magma in the back-arc during Tithonian, as suggested by the >1,000 m-thick sequences of basaltic andesitic lavas of the Río Damas Formation recognized at the Jurassic-Cretaceous boundary in the High Andes of central Chile.

During late Tithonian a new transgression in the Neuquén basin is recorded by the Lo Valdés and Vaca Muerta formations (Klohn, 1960; Legarreta and Uliana, 1999), but no units of this age are observed in Coastal Cordillera, since the upper portion of the Horqueta Formation is eroded (Vergara *et al*., 1995). A possible explanation for this configuration is that the uplift and erosion of the Mesozoic arc continued into the Tithonian, leading to the development of unconformity observed between the Horqueta and Lo Prado Formations (Vergara *et al*., 1995) and Lower Cretaceous granitoids and Lo Prado (Gana and Tosdal, 1996). This is consistent with the presence of numerous zircons of Tithonian age in the Río Damas-Tordillo Formation rocks. The marine transgression originated in the Pacific ocean, since the Atlantic Ocean was not open by the end of the Jurassic, and was facilitated by the progressive ascent of the eustatic level since 160 Ma., which reached its maximum at *ca.* 140 Ma. (Haq *et al*., 1987). The marine transgression occurred through narrow channels that crosscut the arc highlands and connected the ocean with the back-arc basin during Tithonian and Lower Cretaceous, as proposed for Early Jurassic by Vicente (2005).

7. Conclusions

A period of more transpressive conditions in the Andean margin during to the Late Jurassic probably led to the emersion of the arc and fore arc domain, disconnecting the back-arc Mendoza-Neuquén basin from the ocean with a subsequent marine regression phase. The final stage of this regression is recorded by the red clastic deposits of the Río Damas-Tordillo Formation.

Provenance data indicate that an important source of sediments was the uplifted arc domain to the west, represented by Middle to Upper Jurassic granitoids and the Horqueta and Ajial Formations; these are located in the present-day Coastal Cordillera. The supply of sediments from the west continued at least until

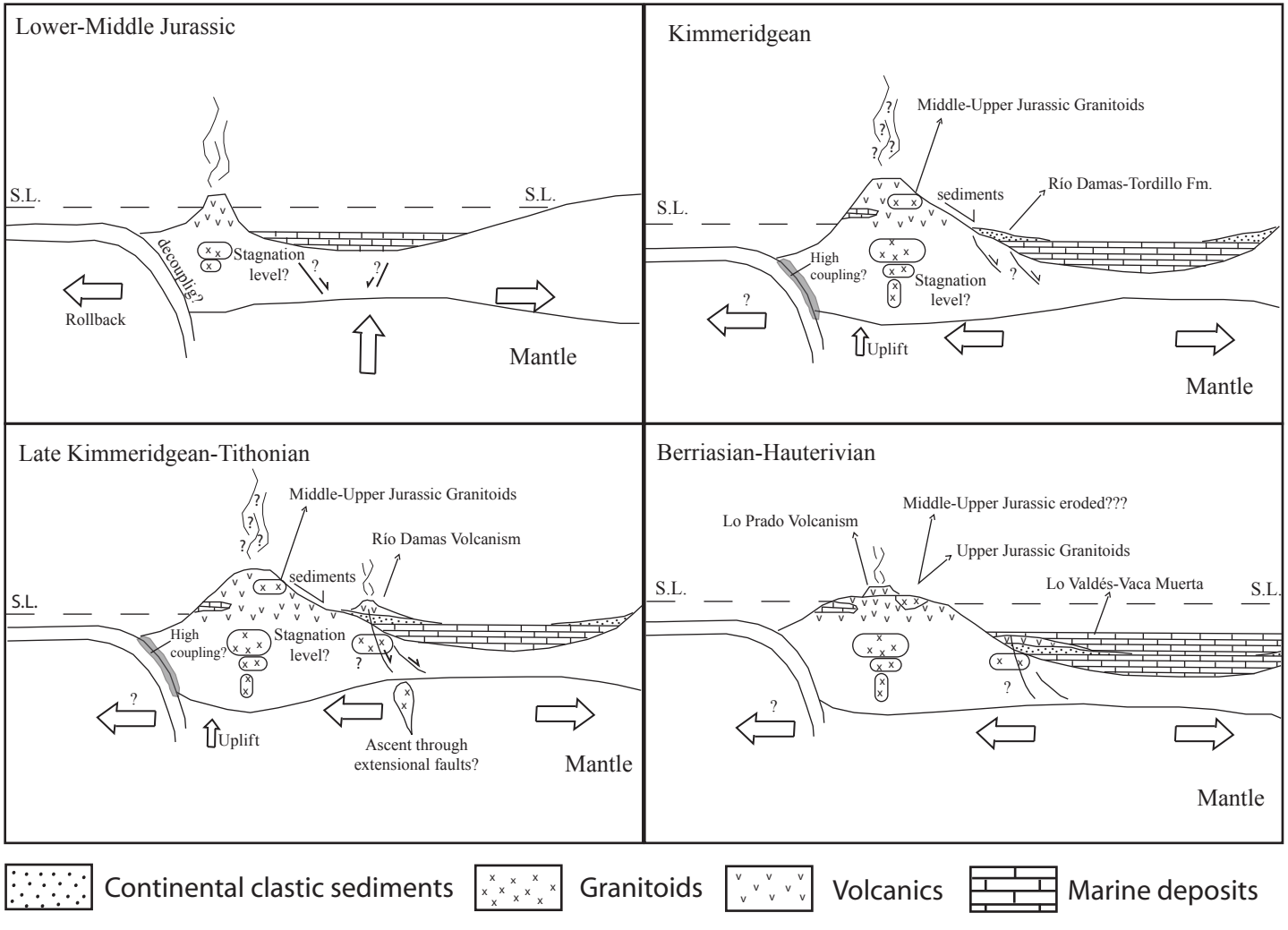

FIG. 13. Jurassic to Early Cretaceous evolution across the western margin of South America between 33° and 35.5°S. **S.L:** Sea Level. White arrows show the direction of the main driving forces acting in the subduction margin.

~146 Ma. The protracted extension in the region since the beginning of the Mesozoic, led to a progressive thinning of the crust, which together with the presence of active normal faults, probably facilitated the rapid ascent of important volumes of lavas in the back-arc during the Kimmeridgian and Tithonian.

The geochemical and isotopic composition of volcanic rocks of the Río Damas-Tordillo Formation indicates a clear subduction-related affinity for the magmatism and points for a depleted sub-arc asthenospheric mantle as the source for the igneous materials. Major and trace elements contents and forward ACF models suggest olivine and plagioclase fractionation combined with small volumes of lower crust assimilation as the main processes controlling magma evolution. Future studies will aim to establish if the source and petrogenetic conditions of the volcanism represented by the Río Damas-Tordillo Formation lavas are different from those of the magmatism in the arc domain.

Acknoledgements

This study was funded by the Fondecyt Nº11080040 and Nº1120272 research grants. Mihai N. Ducea was also funded by grant PN-II-ID-PCE-2011-3-0217 from Romanian UEFISCDI. J. Mescua was founded by PICT-14144 (Agencia Nacional de Promoción Científica y Técnica) y PIP-5843 (CONICET). M. Labbé is thanked for assistance in the field work. S.M. Kay and an anonymous reviewer are thanked for their helpful comments that significantly improved the manuscript.

References

Aguirre, L.; Calderón, S.; Vergara, M.; Oliveros, V.; Morata, D.; Belmar, M. 2009. Edades isotópicas de rocas de los valles Volcán y Tinguiririca, Chile central. *In* Congreso Geológico Chileno, No. 12, Actas S8-001 (digital): 4 p. Santiago.

Biro-Bagoczky, L. 1964. Estudio sobre el límite Titoniano y el Neocomiano en la Formación Lo Valdés, Provincia de Santiago, principalmente en base a ammonoideos, Región Metropolitana, Chile. Memoria de Título (Unpublished), Universidad de Chile, Departamento de Geología: 118 p.

Biro-Bagoczky, L. 1980. Estudio sobre el límite entre el Titoniano y el Neocomiano en la Formación Lo Valdés, provincia de Santiago (33°50'lat. Sur), Chile; principalmente sobre la base de ammonoideos. *In* Congreso Argentino de Paleontología y Bioestratigrafía, No. 2 y Congreso Latinoamericano Paleontología, No. 1, Actas 1: 137-152. Buenos Aires.

Cabanis, B.; Lecolle, M. 1989. Le diagramme La/10-Y/15-Nb/8: un outil pour la discrimination des séries volcaniques at la mise en évidence des processus de mélange et/ou de contamination crustales. Comptes Rendus de l'Academie de Sciences de Paris, série II 309: 2023-2029.

Calderón, S. 2008. Condiciones físicas y químicas del metamorfismo de muy bajo grado de las secuencias mesozoicas en el valle del Río Volcán (33º50'-34º00'S). Memoria de Título (Unpublished), Universidad de Chile, Departamento de Geología: 107 p.

Caminos, R.; Nullo, F.E.; Panza, J.L.; Ramos, V.A. 1993. Mapa Geológico de la provincia de Mendoza. Secretaría de Minería, Dirección Nacional del Servicio Geológico, Buenos Aires, Argentina.

Cegarra, M.I.; Ramos, V.A. 1996. La faja plegada y corrida del Aconcagua. *In* Geología de la región del Aconcagua, provincias de San Juan y Mendoza (Ramos, V.A.; editor). Subsecretaría de Minería de la Nación, Dirección Nacional del Servicio Geológico, Anales 24: 387-422.

Charrier, R. 1981. Geologie der chilenischen Hauptkordillere zwischen 34º und 34º30' südlicher Breite und ihre tektonische, magmatische und paläogeographische Entwicklung. Berliner Geowissenschaftliche Abhandlungen, Reihe A 36: 370 p.

Charrier, R.; Wyss, A.R.; Flynn, J.J.; Swisher, C.; Norell, M.A.; Zapata, F.; McKenna, M.C.; Novacek, M.J. 1996. New evidence for Late Mesozoic-Early Cenozoic evolution of the Chilean Andes in the Upper Tinguiririca Valley (35'S), Central Chile. Journal of South American Earth Sciences 9: 393-422.

Charrier, R.; Pinto, L.; Rodríguez, M.P. 2007. Tectonostratigraphic evolution of the Andean Orogen in Chile. *In* The Geology of Chile (Moreno, T.; Gibbons, W.; editors). The Geological Society: 21-144. London.

Chen, J.H.; Wasserburg, G.J. 1981. The isotopic composition of uranium and lead in Allende inclusions and meteoritic phosphates. Earth and Planetary Science Letters 52: 1-15.

Creixell, C.; Parada, M.A.; Roperch, P.; Morata, D.; Arriagada, C.; Pérez de Arce, C. 2006. Syntectonic emplacement of the Middle Jurassic Concón Mafic Dike Swarm, Coastal Range, central Chile (33ºS). Tectonophysics 425: 101-122.

Creixell, C.; Parada, M.A.; Morata, D.; Roperch, P.; Arriagada, C. 2009. The genetic link between mafic dike swarms and plutonic reservoirs in the Mesozoic

of central Chile (30º-33º45'S): insights from AMS and geochemistry. International Journal of Earth Sciences 98: 177-201.

Creixell, C.; Parada, M.A.; Morata, D.; Vásquez, P.; Pérez de Arce, C.; Arriagada, C. 2011. Middle-Late Jurassic to Early Cretaceous transtension and transpression during arc building in central Chile: evidence from mafic dike swarms. Andean Geology 38 (1): 37-63. doi: 10.5027/andgeoV38n1-a04

Cucchi, R.; Leanza, H.A.; Repol, D.; Escosteguy, L.; González, R.; Daniela, J.C. 2005. Hoja Geológica 3972-IV, Junín de los Andes. Provincia del Neuquén. Instituto de Geología y Recursos Minerales, Servicio Geológico Minero Argentino, Boletín 357: 102 p.

Davidson, J. 1971. Geología del área de las Nacientes del Teno, provincia de Curicó, Chile. Memoria de Título (Unpublished), Universidad de Chile, Departamento de Geología: 160 p.

Davidson, J.; Vicente, J.C. 1973. Características paleogeográficas y estructurales del área fronteriza de las nacientes del Teno (Chile) y Santa Elena (Argentina) (Cordillera Principal, 35° a 35°15'latitud sur). *In* Congreso Geológico Argentino, No. 5, Actas 5: 11-55. Buenos Aires.

DePaolo, D.J. 1981. Trace element and isotopic effects of combined wallrock assimilation and fractional crystallization. Earth and Planetary Science Letters 53: 189-202.

Deckart, K.; Hervé, F.; Fanning, C.M.; Ramírez, V.; Calderón, M.; Godoy, E. 2014. U-Pb geochronology and Hf-O isotopes of zircons from the Pennsylvanian Coastal Batholith, south-central Chile. Andean Geology 41 (1): 49-82. doi: 10.5027/andgeoV41n1-a03

Drew, S.T.; Ducea, M.N.; Schoenbohm, L.M. 2009. Mafic volcanism on the Puna Plateau, NW Argentina: Implications for lithospheric composition and evolution with an emphasis on lithospheric foundering: Lithosphere 1: 305-318. doi: 10.1130/L54.1.

Faure, G. 1986. Principles of Isotope Geochemistry. John Wiley: 464 p. New York.

Faure, G.; Mensing, T.M. 2005. Isotopes: Principles and Applications. John Wiley: 928 p. New York.

Gana, P.; Tosdal, R. 1996. Geocronología U-Pb y K-Ar en intrusivos del Paleozoico y Mesozoico de la Cordillera de la Costa, Región de Valparaíso, Chile. Revista Geológica de Chile 23 (2): 151-164. doi: 10.5027/andgeoV23n2-a04

Gehrels, G.E.; Valencia, V.A.; Ruiz, J. 2008. Enhanced precision, accuracy, efficiency, and spatial resolution of U-Pb ages by laser ablation-multicollector-inductively coupled plasma-mass spectrometry. Geochemistry, Geophysics, Geosystems 9: Q03017. doi: 10.1029/2007GC001805.

Giambiagi, L.B.; Álvarez, P.; Godoy, E.; Ramos, V.A. 2003. The control of preexisting extensional structures on the evolution of the southern sector of the Aconcagua fold and thrust belt, southern Andes. Tectonophysics 369: 1-19.

Godoy, E.; Loske, W. 1988. Tectonismo sinplutónico de dioritas Jurásicas al sur de Valparaíso: datos U-Pb sobre la 'fase Quintay'. Revista Geológica de Chile 15 (2): 119-127. doi: 10.5027/andgeoV15n2-a02

González, O. 1963. Observaciones geológicas en el valle del Río Volcán. Revista Minerales 17 (81): 20-61. Santiago.

Grocott, J.; Taylor, G.K. 2002. Magmatic arc fault systems, deformation partitioning and emplacement of granitic complexes in the Coastal Cordillera, north Chilean Andes (25°30'S to 27°00'S). Journal of the Geological Society 159 (4): 425-442.

Hallam, A.; Biro-Bagoczky, L.; Pérez, E. 1986. Facies analysis of the Lo Valdés Formation of the High Cordillera of central Chile, and the paleogeographic evolution of the Andean basin. Geological Magazine 123 (4): 425-435.

Haq, B.U.; Hardenbol, J.; Vail, P.R. 1987. Chronology of fluctuating sea levels since the Triassic (250 million years ago to present). Science 235: 1156-1167.

Hart, S.R. 1984. A large-scale isotope anomaly in the Southern Hemisphere mantle. Nature 309: 753-757.

Hervé, F.; Munizaga, F.; Parada, M.A.; Brook, M.; Pankhurst, R.; Snelling, N.; Drake, R. 1988. Granitoids of the Coast Range of central Chile: geochronology and geologic setting. Journal of South American Earth Sciences 1: 185-194.

Hildreth, W.; Moorbath, S. 1988. Crustal contribution to the arc magmatism in the Andes of central Chile. Contribution to Mineralogy and Petrology 103: 361-386.

Howell, J.A.; Schwarz, E.; Spalletti, L.A.; Veiga, G.D. 2005. The Neuquén Basin, Argentina: An Overview. *In* The Neuquén Basin: a case study in sequence stratigraphy and basin dynamics (Veiga, G.D.; Spalletti, L.A.; Howell, J.A.; Schwarz, E.; editors). Geological Society of London, Special Publications 252: 1-14.

Klohn, C. 1960. Geología de la Cordillera de los Andes de Chile Central, Provincias de Santiago, O'Higgins, Colchagua y Curicó. Instituto de Investigaciones Geológicas, Boletín 8: 95 p. Santiago.

Kramer, W.; Siebel, W.; Romer, R.; Haase, G.; Zimmer, M.; Ehrlichmann, R. 2004. Geochemical and isotopic characteristics and evolution of the Jurassic volcanic

arc between Arica (18°30'S) and Tocopilla (22°S), North Chilean Coastal Cordillera. Chemie der Erde 65: 47-78.

Leanza, H.A. 1981. The Jurassic-Cretaceous boundary beds in west central Argentina and their ammonite zones. Neues Jahrbuch für Geologie und Paläontologie, Abhandlungen 161: 62-92. Stuttgart.

Leanza, H.A.; Hugo, C. 1997. Hoja Geológica 3969-III. Picún Leufú. Provincias de Neuquén y Río Negro. Servicio Geológico Minero Argentino, Boletín 218: 135 p.

Legarreta, L. 1976. Análisis estratigráfico de la Formación Tordillo (Kimmeridgiano superior) entre el Río Diamante y el Río Salado, Departamentos de San Rafael y Malargue, Provincia de Mendoza, Argentina. Tesis (Unpublished), Universidad de Buenos Aires, Departamento de Geología: 72 p.

Legarreta, L.; Uliana, M.A. 1999. El Jurásico y Cretácico de la Cordillera Principal y la cuenca Neuquina. 1. Facies sedimentarias. *In* Geología Argentina (Caminos, R.; editor). Servicio Geológico y Minero Argentino, Instituto de Geología y Recursos Minerales, Anales 29 (16): 399-416.

Legarreta, L.; Gulisano, C.A.; Uliana, M.A. 1993. Las secuencias sedimentarias jurásico-cretácicas. *In* Geología y Recursos Naturales de Mendoza (Ramos, V.A.; editor). Congreso Geológico Argentino, No. 12 y Congreso de Exploración de Hidrocarburos, No. 2, Relatorio: 87-114. Buenos Aires.

Levi, B.; Aguirre, L.; Nyström, J.O.; Padilla, H.; Vergara, M. 1989. Low-grade regional metamorphism in the Mesozoic-Cenozoic volcanic sequences of the Central Andes. Journal of Metamorphic Geology 7: 487-495.

Le Maitre, R.W. 1989. A classification of igneous rocks and glossary of terms. Blackwell Scientific Publication: 193 p. London.

López-Gómez, J.; Martín-Chivelet, J.; Palma, R.M. 2009. Architecture and development of the alluvial sediments of the Upper Jurassic Tordillo Formation in the Cañada Ancha Valley, northern Neuquén Basin, Argentina. Sedimentary Geology 219: 180-195.

Lucassen, F.; Franz, G. 1994. Arc related Jurassic igneus and meta-igneus rocks in the Coastal Cordillera of northern Chile/ Region Antofagasta. Lithos 32: 273-298.

Lucassen, F.; Escayola, M.; Romer, R.; Voramonte, J.; Koch, K.; Franz, G. 2002. Isotopic composition of Late Mesozoic basic and ultrabasic rocks from the Andes (23-32°S) implications for the Andean mantle. Contributions to Mineralogy and Petrology 143: 336-349.

Lucassen, F.; Kramer, W.; Bartsch, V.; Wilke, H.G.; Franz, G.; Romer, R.L.; Dulski, P. 2006. Nd, Pb and Sr isotope composition of juvenile magmatism in the Mesozoic large magmatic province of northern Chile (18°-27°S): indications for a uniform subarc mantle. Contributions to Mineralogy and Petrology 152: 571-589.

Ludwig, K.R. 2003. User's manual for isoplot 3.00: A geochronological toolkit for Microsoft Excel. Berkeley Geochronological Center, Special Publication 4: 71 p. Berkeley, California.

Martínez, F.; Arriagada, C.; Mpodozis, C.; Peña, M. 2012. The Lautaro Basin: A record of inversion tectonics in northern Chile. Andean Geology 39 (2): 258-278. doi: 10.5027/andgeoV39n2-a04

Mescua, J.F. 2011. Evolución estructural de la cordillera principal entre Las Choicas y Santa Elena (35ºS), provincia de Mendoza, Argentina. Tesis (Unpublished), Universidad de Buenos Aires: 241 p.

Mescua, J.F.; Giambiagi, L.B.; Bechis, F. 2008. Evidencias de tectónica extensional en el Jurásico tardío (Kimeridgiano) del suroeste de la provincia de Mendoza. Revista de la Asociación Geológica Argentina 63 (4): 512-519.

Mescua, J.F.; Giambiagi, L.B.; Ramos, V. 2012. Late Cretaceous Uplift in the Malargüe fold-and-thrust belt (35°S), southern Central Andes of Argentina and Chile. Andean Geology 40 (1): 102-116. doi: 10.5027/andgeoV40n1-a05

Mpodozis, C.; Ramos, V. 2008. Tectónica Jurásica en Argentina y Chile: Extensión, subducción oblicua, rifting, deriva y colisiones? Revista de la Asociación Geológica Argentina 63 (4): 481-497.

Muñoz, M.; Deckart, K.; Charrier, R.; Fanning, M. 2009. New geochronological data on Neogene-Quaternary intrusive rocks from the high Andes of central Chile (33º15'-34º00'S). *In* Congreso Geológico Chileno, No. 12, Resúmenes, Sesión 8-008: 4 p. Santiago.

Naipauer, M.; García, E.; Marques, J.; Tunik, M.; Rojas, E.; Vujovich, G.; Pimentel, M.; Ramos, V. 2012. Intraplate Late Jurassic deformation and exhumation in western central Argentina: Constraints from surface data and U-Pb detrital zircon ages. Tectonophysics 524-525: 59-75.

Naipauer, M.; Tunik, M.; Marques, J.C.; Rojas, E.; Vujovich, G.; Pimentel, M.; Ramos, V. 2014. U-Pb detrital zircon ages of Upper Jurassic continental succcessions: implications for the provenance and absolute age of the Jurassic-Cretaceous boundary in the Neuquén Basin. Geological Society Special Publication: 399. doi: 10.1144/SP399.1.

Oliveros, V.; Féraud, G.; Aguirre, L.; Fornari, M.; Morata, D. 2006. The Early Andean Magmatic Province (EAMP):

$^{40}Ar/^{39}Ar$ dating on Mesozoic volcanic and plutonic rocks from the Coastal Cordillera, Northern Chile. Journal of Volcanology and Geothermal Research 157: 311-330.

Oliveros, V.; Morata, D.; Aguirre, L.; Féraud, G.; Fornari, M. 2007. Jurassic to Early Cretaceus subduction-related magmatism in the Coastal Cordillera of northern Chile (18°30'-24°S): geochemistry and petrogenesis. Revista Geológica de Chile 34 (2): 209-232. doi: 10.5027/andgeoV34n2-a03

Oliveros. V.; Aguirre, L.; Morata, D.; Simonetti, A.; Vergara, M.; Belmar, M.; Calderón, S. 2008. Geochronology of very low-grade mesozoic andean metabasites. An approach through the K-Ar, $^{40}Ar/^{39}Ar$ and U-Pb LA-MC-ICP-MS methods. Journal of the Geological Society 165: 579-584.

Oliveros, V.; Labbé, M.; Rossel, P.; Charrier, R.; Encinas, A. 2012. Late Jurassic paleogeographic evolution of the Andean back-arc basin: new constrains from the Lagunillas Formation, northern Chile (27º30'-28º30'S). Journal of South American Earth Sciences 35: 25-40.

Otamendi, J.; Ducea, M.N.; Tibaldi, A.; de la Rosa, J.; Bergantz, G.; Vujovich, G. 2009. Generation of tonalitic and dioritic magmas by coupled partial melting of gabbroic and metasedimentary rocks within the deep crust of the Famatinian magmatic arc, Argentina. Journal of Petrology 50: 841-873. doi: 10.1093/petrology/egp022.

Pángaro, F.; Ramos, V.A.; Godoy, E. 1996. La faja plegada y corrida de la Cordillera Principal de Argentina y Chile a la latitud del Cerro Palomares (33°35'S). *In* Congreso Geológico Argentino, No. 13 y Congreso Exploración de Hidrocarburos, No. 3, Actas 2: 315-324. Buenos Aires.

Parada, M.A.; Nystrom, J.; Levi, B. 1999. Multiple sources for the Coastal batholith of central Chile (31-34°S): geochemical and Sr-Nd isotopic evidence and tectonic implications. Lithos 46: 505-521.

Pearce, J.A. 1982. Trace elements characteristics of lavas from destructive plate boundaries. *In* Andesites (Thorpe, R.S.; Editor). John Wiley and Sons: 525-548. London.

Pearce, J.A. 1983. Role of the sub-continental lithosphere in magma genesis at active continental margins. *In* Continental basalts and mantle xenoliths (Hawkesworth, C.J.; Norry, M.J.; editors). Shiva, Nentwich: 230-249.

Pearce, J.A. 1996. A user's guide to basalt discrimination diagrams. *In* Trace element geochemistry of volcanic rocks, applications for massive sulphide exploration, Short Course Notes. (Bailes, A.H.; Christiansen, E.H.; Galley, A.G.; Jenner, G.A.; Keith, Jeffrey D.; Kerrich, R.; Lentz, D.R.; Lesher, C.M.; Lucas, S.B.; Ludden, J.N.; Pearce, J.A.; Peloquin, S.A.; Stern, R.A.; Stone, W.E.; Syme, E.C.; Swinden, H.S.; Wyman, D.A.; editors). Geological Association of Canada 12: 79-113.

Peate, D.W.; Pearce, J.A.; Hawkesworth, C.J.; Colley, H.; Edwards, C.M.H.; Hirose, K. 1997. Geochemical variations in Vantu arc lavas: the role of subducted materials and a variable mantle wedge composition. Journal of Petrology 38: 1331-1358.

Plank, T. 2005. Constraints from Thorium/Lanthanum on sediments recycling at subduction zones and the evolution of continents. Journal of Petrology 46: 921-944.

Riccardi, A.C. 2008a. The marine Jurassic of Argentina: a biostratigraphic framework. Episodes 31 (3): 326-335.

Riccardi, A.C. 2008b. El Jurásico de la Argentina y sus amonites. Revista de la Asociación Geológica Argentina 63 (4): 625-643.

Ring, U.; Willner, A.; Layer, P.; Richter, P. 2012. Jurassic to Early Cretaceous postaccretional sinistral transpression in northcentral Chile (latitudes 31-32°S). Geological Magazine 149 (2): 202-220.

Robinson, D.; Bevins, R.; Aguirre, L.; Vergara, M. 2004. A reappraisal of episodic burial metamorphism in the Andes of central Chile. Contributions to Mineralogy and Petrology 146: 513-528.

Rossel, P.; Oliveros, V.; Ducea, M.; Charrier, R.; Scaillet, S.; Retamal, L.; Figueroa, O. 2013. The Early Andean subduction system as an analogue to island arcs: evidence from across-arc geochemical variations in northern Chile. Lithos 179: 211-230.

Rudnick, R.L.; Gao, S. 2003. Composition of the continental crust. *In* The Crust (Rudnick, R.L.; editor). Elsevier 3: 1-64.

SERNAGEOMIN. 2003. Mapa Geológico de Chile: versión digital. Servicio Nacional de Geología y Minería, Publicación Geológica Digital, No. 4 (CD-ROM, versión1.0, 2003). Santiago.

Scheuber, E.; González, G. 1999. Tectonics of the Jurassic-Early Crataceous magmatic arc of the north Chilean Coastal Cordillera (22°-26°S): A story of crustal deformation along a convergent plate boundary. Tectonics (18): 895-910.

Stacey, J.S.; Kramers, J.D. 1975. Approximation of terrestrial lead isotope evolution by a two-stage model. Earth and Planetary Science Letters 26, 207-221. doi: 10.1016/0012-821X(75)90088-6.

Stern, C.R. 1991. Role of subduction erosion in the generation of the Andes magmas. Geology 19: 78-81.

Stern, C.R. 2011. Subduction erosion: Rates, mechanism, and its role in arc magmatism and the evolution of the

continental crust and mantle. Gondwana Research 20: 284-308.

Spalletti, L.A.; Queralt, I.; Matheos, S.D.; Colombo, F.; Maggi, J. 2008. Sedimentary petrology and geochemistry of siliciclastic rocks from the upper Jurassic Tordillo Formation (Neuquén Basin, western Argentina): Implications for provenance and tectonic setting. Journal of South American Earth Sciences 25: 440-463.

Stipanicic, P.N. 1965. El Jurásico en Vega de la Veranada (Neuquén). El Oxfordense y el diastrofismo divesiano (Agassiz-Yaila) en Argentina. Revista de la Asociación Geológica Argentina 20 (4): 403-478. Buenos Aires.

Stipanicic, P.N. 1969. El avance en los conocimientos del Jurásico argentino a partir del esquema de Groeber. Revista de la Asociación Geológica Argentina 24 (4): 367-388. Buenos Aires.

Sun, S.S.; McDonough, W.F. 1989. Chemical and isotopic systematics of oceanic basalts: implications for mantle composition and processes. Geological Society Special Publication 42: 313-345.

Thibodeau, A.M.; Killick, D.J.; Ruiz, J.; Chesley, J.T.; Deagan, K.; Cruxent, J.M.; Lyman, W. 2007. The strange case of the earliest silver extraction by European colonists in the New World. Proceedings of the National Academy of Sciences of the United States of America 104: 3663-3666.

Thiele, R. 1980. Hoja Santiago, Región Metropolitana. Servicio Nacional de Geología y Minería, Carta Geológica de Chile 39: 51 p.

Vergara, M.; Levi, B.; Nystrom, J.; Cancino, A. 1995. Jurassic and Early Cretaceous island arc volcanism, extension, and subsidence in the Coast Range of central Chile. Geological Society of America Bulletin 107: 1427-1440.

Vicente, J.C. 2005. Dynamic paleogeography of the Jurassic Andean Basin: pattern of transgression and localization of main straits through the magmatic arc. Revista de la Asociación Geológica Argentina 60 (1): 221-250.

Vicente, J.C. 2006. Dynamic Paleogeography of the Jurassic Andean Basin: pattern of regression and general considerations on main features. Revista de la Asociación Geológica Argentina 61: 408-437.

Weaver, C.E. 1931. Paleontology of the Jurassic and Cretaceous of West Central Argentina. University of Washington, Memoir 1: 1-469. Seattle.

Winchester, J.A.; Floyd, P.A. 1977. Geochemical discrimination of different magma series and their differentiation products using immobile elements. Chemical Geology 20: 325-343.

Yrigoyen, M.R. 1979. Cordillera Principal. *In* Segundo Simposio de Geología Regional Argentina (Turner, J.C.M.; coordinador). Academia Nacional de Ciencias: I65l-I694.

Zavala, C.; Martínez Lampe, J.; Fernández, M.; Di Meglio, M.; Ancuri, M. 2008. El Diacronismo entre las formaciones Tordillo y Quebrada del Sapo (Kimeridgiano) en el sector sur de la Cuenca Neuquina. Revista de la Asociación Geológica Argentina 63 (4): 754-765. Buenos Aires.

Manuscript received: October 24, 2013; revised/accepted: June 3, 2014; available online: June 3, 2014.